EUROPEAN COMMISSION

Community Research

SEVENTH FRAMEWORK PROGRAMME

CARBOWASTE

Treatment and Disposal of Irradiated Graphite and Other Carbonaceous Waste

Grant Agreement Number: FP7-211333

Technical Report T-3.3.2-a

Autoradiographic Investigations of Reactor Graphite before Treatment

Author(s):

Markus Baier

Fachhochschule Aachen – Forschungszentrum Jülich

Document Number: CARBOWASTE-1203-T-3.3.2-a
Date of issue of this report: 30/03/2012

Project co-funded by the European Commission under the Seventh Framework Programme (2007 to 2011) of the European Atomic Energy Community (EURATOM) for nuclear research and training activities		
Dissemination Level		
PU	Public	
RE	Restricted to the partners of the CARBOWASTE project	
CO	Confidential, only for specific distribution list defined on this document	**X**

Start date of project: **01/04/2008** Duration: **48 Months**

Distribution list

Person and organisation name and/or group	Comments
WP3 members	
Executive Board	
Co-ordinator	
CARBOWASTE-All	

CARBOWASTE		
Work package: 3 **Task:** 3.3	**CARBOWASTE document no:** CARBOWASTE-1203-T-3.3.2-a	**Document type:** T=Technical Report
Issued by: Fachhochschule Aachen – Forschungszentrum Jülich (DE) **Internal no.:** CW1203-T-3-3-2-a		**Document status:** Final

Document title

Autoradiographic Investigations of Reactor Graphite before Treatment

Executive summary

In the context of a student research project, autoradiographic investigations of reactor graphite were undertaken. Five graphite samples (MERLIN, DIDO, AVR, SLA and RBMK) of different reactors (FRJ-1, FRJ-2, HTR, UNGG and RBMK) were used. The autoradiographic measurements were made with an Instant Imager. Self-made aluminium filters (six different thicknesses) were put between the graphite sample and the Instant Imager detection system. The resulting images of the samples showed mostly a homogenous distribution of the radionuclides. The images of the RBMK sample show area of a circled radionuclide concentration. The effect of the aluminium absorbers decreases with increasing aluminium thickness. It is expected that H-3 and C-14 radiation is mostly absorbed by the aluminium filters. For more detailed information about the radionuclide distribution the measurement method must be improved.

Revisions

Rev.	Date	Short description	Author	Internal Review	Task Leader	WP Leader
00	dd/mm/yyyy	Issue	Name, Organisation	Name, Organisation *Signature*	Name, Organisation *Signature*	Name, Organisation *Signature*
01	15/11/2011	First issue	Baier FH Aachen	von Lensa FZJ	Vulpius FZJ	Piña CIEMAT
02	19/03/2012	Final Issue	Baier FH Aachen	von Lensa FZJ	Vulpius FZJ	Piña CIEMAT

Table of Content

1 Motivation

This work is part of the CARBOWASTE project, which was started in 2008 under the 7th EURATOM Framework Program. In this program several international companies, authorities, universities and research centers try to develop best practices in the retrieval, characterization, treatment and disposal of irradiated graphite, so called i-graphite.

The aim of this work is finding out the distribution (homogeneous or heterogeneous) of the radionuclide inventory in graphite samples from several reactors (AVR, DIDO, RBMK, MERLIN and SLA). Because of neutron activation of the natural C-13 or impurities within the graphite or coolant the i-graphite contains H-3, C-14, Cl-36, Co-60, Cs-137 and Sr-90/Y-90. With absorbing aluminum filters of different thicknesses autoradiographic images of the samples were taken and analyzed with an image processing software (ImageJ).

2 Reactor graphite

Carbon is a nonmetal of group 14 of the periodic table of elements. There are approximately $2 \cdot 10^6$ artificially produced and naturally occurring compounds of carbon. For other elements of the periodic table there are not more than 10000. Carbon is an important part for living organisms (RNA, DNA) [Fro 04]. In nature carbon exists in two modifications. As metastable diamant and as stable graphite [Sap 79]. Graphite can be used for example as an electrode for lithium ion battery [Tuc 03] or as material for nuclear propulsion systems in space applications [Gul 64].

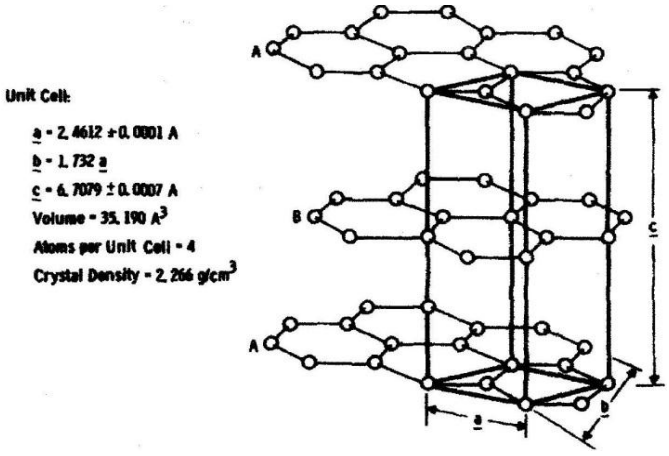

Figure 1: Crystal structure of graphite [Bak 70].

Another field of application is in nuclear reactors where it is used often as reflector and/or moderator material [DIP 04].

2.1 Structure, properties and radionuclide inventory

Most commonly graphite exists in the hexagonal lattice structure, as shown in Figure 1. The stacking sequence is ABAB, whereas it is ABCABC for the not so common rhombohedral structure. Most properties of graphite can be related to two structural features.

The strong chemical bonds resulting in mobile electrons responsible for thermal/electric conductivity for instance. Additionally the large spacing between two structure layers affects mechanical characteristics.

Mechanical properties like creeping, compressive strength, young`s modulus, coefficient of friction or the tensile strength are discussed in [Bak 70] and [Röd 76]. The tensile strength for example increases with temperature and reaches its maximum at some 2500 °C. It depends on the particle size and the processing parameters for instance.

Thermal properties, like the thermal conductivity, depend on temperature too. The conductivity is e.g. a function of the type of the graphite and the production variables. The maximum is for nuclear graphite below room temperature and decreases at elevated temperatures. Further thermal characteristics, like thermal expansion and emissivity, are object in [Bak 70].

The nuclear properties, are excellent for using graphite as moderator and reflector material for instance. It has a low thermal neutron absorption cross section and a high scattering cross section. Impurities, like H, B, N, Cl or other rare elements, change the positive nuclear characteristics. They increase, for instance, the absorption cross section for neutrons.

Impurities develop corrosion processes in the graphite and adulterate the neutron economy of the reactor. The purity of graphite is given as the amount of ash in combustion analysis [Mer 69]. In normal, pure graphite it is 1000 ppm and more, whereas it is 50-350 ppm for graphite used in reactors. As in this work a sample of an AVR reactor is used in table 1 the impurity inventory of a graphite sample called “reactor grade” is shown. This sample was produced by

the US company Union Carbide Corporation. After [Mer 69] it has the same quality like the graphite used in the AVR reactor for the fuel elements.

Table 1: Trace impurities in the sample „reactor grade“ in [ppm].

Sodium	Bromine	Copper	Tellurium	Lanthanum	Thorium	Uranium
9	1.2	1.3	20.6	0.1	0.07	< 0.05

[Bro 01] and [Bus 02], for instance, deal also with the chemical inventory of graphite and its impurities.

2.2 Types

Different nuclear graphites can be generated by changing parameters, like temperature or grain size, in the production process. These nuclear graphite grades can differ in purity, strength, density, processing conditions or piece size for example. In literature the graphite types are named with manufacturer letters and the number designation, like NBG-10 (NBG = Nuclear Block Graphite) [Bak 70], [Sgl 01]. In [Moo 08], [Hop 03], [Vre 08], [Bak 70] and [Ish 04] graphite grades and designations for components in differing reactor types are shown. Companies producing and selling such graphites for the nuclear industry are for example SGL, GrafTech (both Europe) and Toyo Tanso (Japan) [Vre 08].

2.3 Manufacturing

Graphite is a special form of carbon. To create carbon or graphite products the pyrolytic decomposition is mostly used. Nuclear graphite is a highly pure kind of electrographite. Electrographites are materials at which the carbon is heat treated (graphitized) at temperatures greater than 2200 °C [BAK 70]. After [Haa 90] with the Acheson process most of the nuclear graphite was produced. In figure 2 are similar steps shown for producing nuclear graphite out of the raw material petroleum coke.

The first processing step is the calcination. With it the volatile hydrocarbons are removed. Additionally the calcination preshrinks the coke for a better volume control in the production process which is important for large graphite blocks.

It follows the crushing of the calcined coke. The crushed coke is then milled to a flour which is mixed with coke filler particles forming a blend. Pitch binder is added at a temperature of 165 °C to the blend. The fluid mixture is now extruded. The anisotropy property of graphite is result of the parallel alignment of the coke particles relative to the direction of extrusion. If molding is used the coke particles align perpendicular to the extrusion direction. The alignment of the coke particles is responsible for the strength of the graphite and depends on the forming method [Sri 08].

Now a heating up is done. The present "green" carbon bars are packed in granulate coke for maintaining the shape and then heated up to 800 °C. This leads to a conversion of pitch from a thermoplastic state to an infusible solid. The heating up must be done slowly (3 to 6 weeks). Otherwise the production of hydrocarbon gases can create cracks in the graphite bars.

Impregnating or graphitizing closes the production cycle. Either the baked article can graphitize directly or, what is done mostly, it is impregnated with pitch. The impregnation reduces the porosity of the graphite and increases the bulk density. For this the graphite bars are brought into an electric graphitizing furnace fired at 2600 °C to 3000°C. The heating cycle lasts 3 to 4 days. The following cooling lasts 10 days to decrease the number of microcracks [Sri 08]. Finally the graphite comes in touch with air. Thermal (heating to 2800 °C or 3000 °C) or chemical (heating in presence of halogen containing gases) purity improvements can follow.

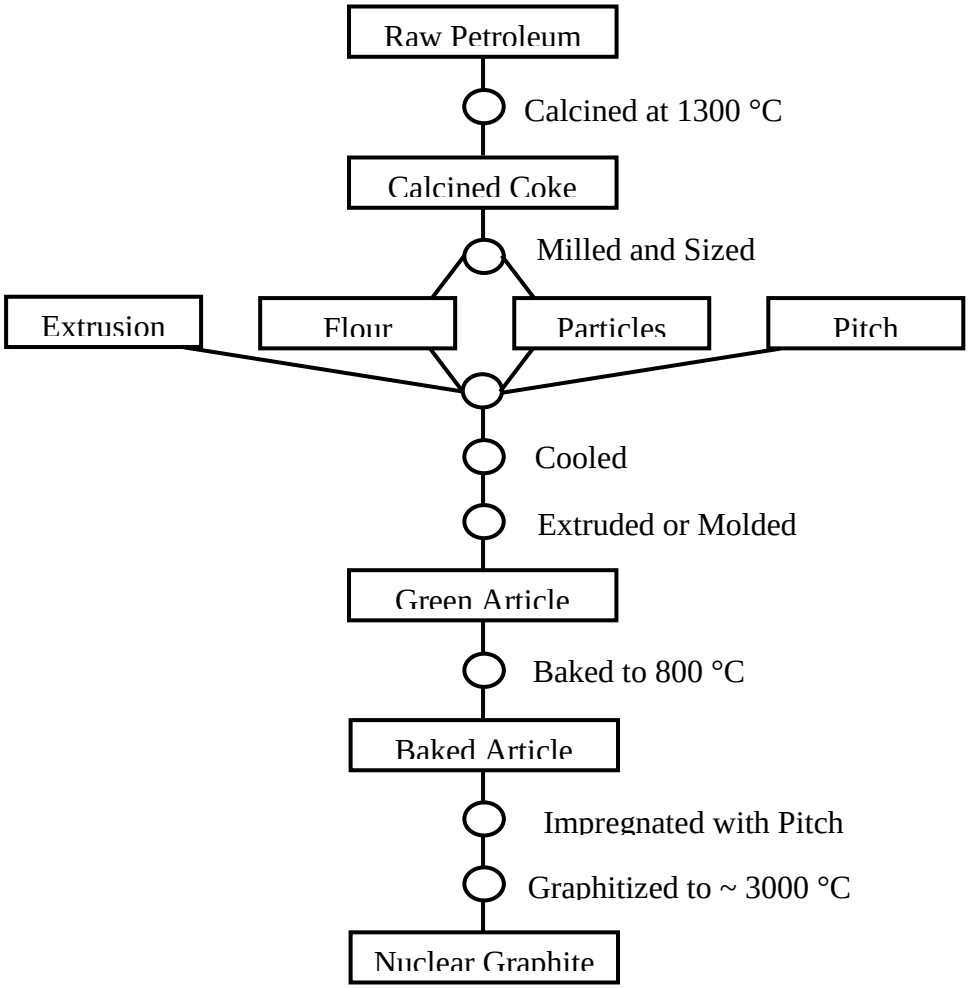

Figure 2: Steps for manufacturing nuclear graphite [Bak 70].

2.4 Graphite components and reactor types

Graphite is a popular material for nuclear purposes. It has a high mechanical strength, very good moderating characteristics and a low neutron absorption cross-section [Agr 61]

Hence it is used very often as a material for the moderator. In the Russian RBMK the bricks for the fuel channel [Hop 03] and solid-contact rings [Leb 98] are made out of graphite for instance. According to [Fro 04] there are some 1000 – 2500 tons of graphite in such a reactor type in average. Matrix material for fuel elements and absorbing rods are for example in a high-temperature gas-cooled reactor (HTGCR) also of graphite.

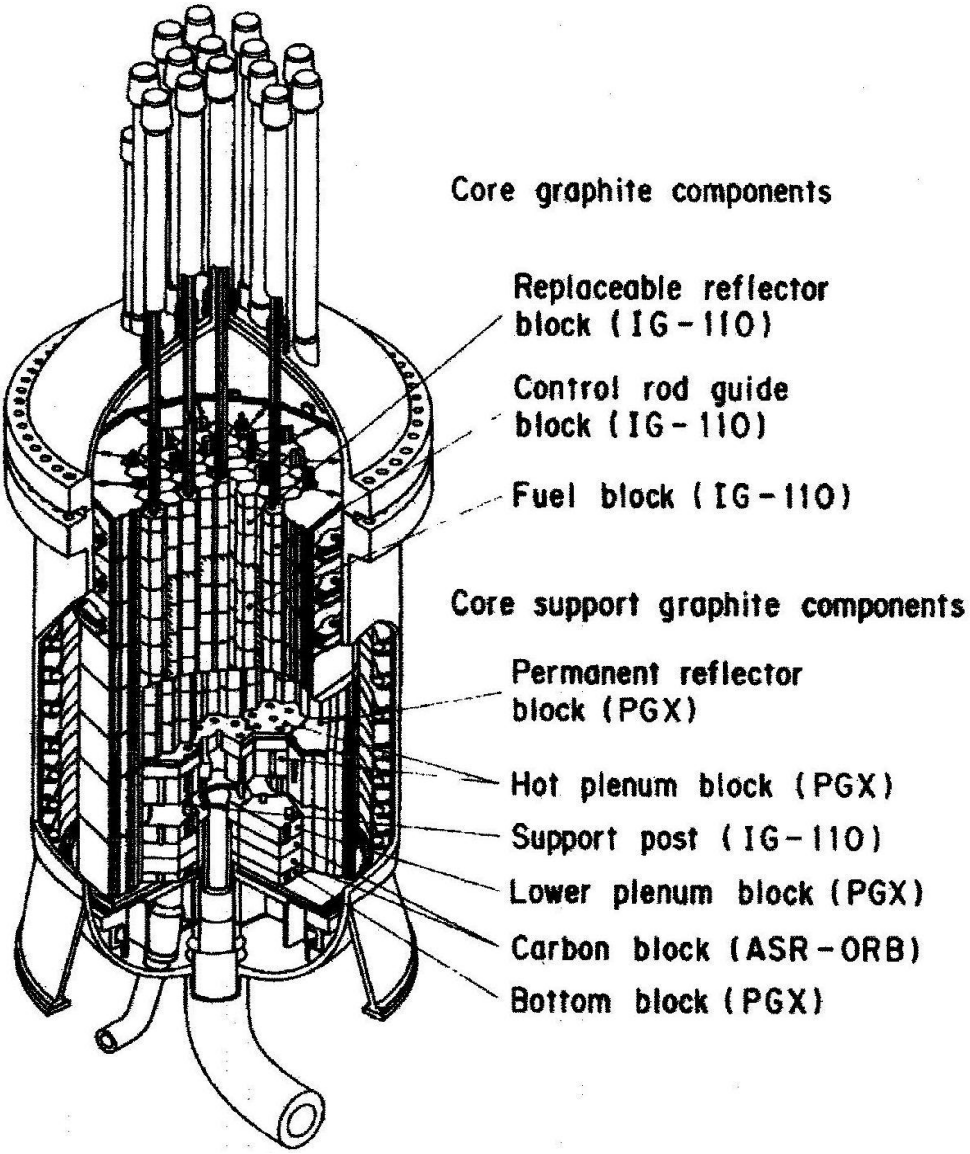

Figure 3: Graphite components in a High Temperature Engineering Test Reactor (HTTR) with used graphite grades in brackets [Ish 04].

The low absorption cross-section for neutrons is also appropriate for reflectors like in high-power water-graphite channel reactor for instance [Leb 98]. Figure 3 indicates the role of graphite for replaceable components and for permanently installed graphite components of the reactor core [Ish 04]. In [Vre 08] the usage of graphite in a High Temperature Reactor (HTR) is mentioned. Graphite is also part of British Magnox reactors [Mcg 11], French uranium natural graphite gaz reactors (UNGG), English advanced gas reactors (AGR) [Gui 10], [Nei 07], Russian light water-cooled graphite moderated (LWGR) reactors [Ia1 06] or of some research reactors like in the ASTRA research reactor in Austria [Lex 06].

Finally it is worth to mention, that also in tokamak fusion reactors graphite or chemical compounds with graphite [Fuk 85] play an important role. Graphite offers excellent thermal properties, a high sublimation temperature, a high heat capacity and a high thermal conductivity [Cau 89]. Graphite can be used for plasma facing components in a tokamak fusion reactor. They are used as material for fixed and movable limiters forming the plasma column [Che 94].

2.5 Irradiation behaviour

Not only impurities are able to change the properties of graphite but also the neutrons in form of irradiation during the operation in a nuclear power plant.

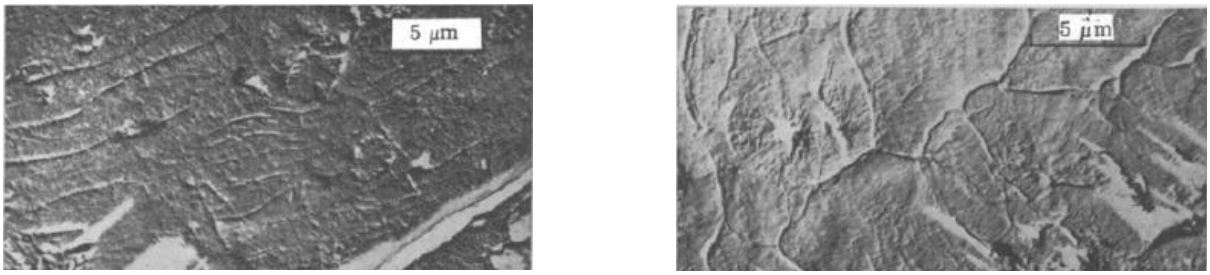

Figure 4: Left: Graphite before irradiation. Right: Cracks in graphite after irradiation ($T_{irr} = 500°C, neutron\ fluence: 5 \cdot 10^{21} neutrons/cm^2$)[Agr 61].

The development of radiation induced effects, resulting in property changes of the material, start with primary radiation damage. These point defects in the lattice create at the microcrystallite level oriented microstructures ending in shape changes. Geometrical changes

generate microstresses which are responsible for the porous subsystem of graphite. Finally microstructural developments take place [Sub 06].

Microcracks (see figure 4 and figure 5) evolve because of the irradiation and they are the main reason for the observed radiation effects [Pan 08].

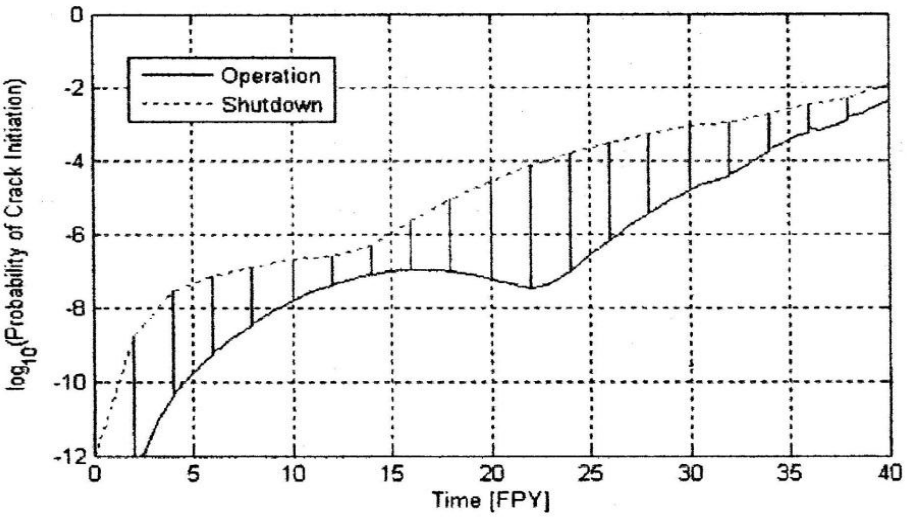

Figure 5: Probability for crack initiation during operation life [Nei 07].

In-pile exposure results in an alteration of the crystal structure and hence property changes occur. From the practical point of view the most important effects on graphite are the reduction of thermal conductivity, the storing of latent energy (Wigner) and the dimensional instability of graphite components [Kli 61]. The dimensional instabilities depend on the temperature and the neutron flux. Up to irradiation temperatures of 300 °C there is swelling and between temperatures of 500 and 800 °C there is shrinkage of the graphite material [Agr 61]. In [Eng 84] the behaviour of different types of graphite (highly oriented pyrolytic graphites and artificial polycrystalline graphites) in respect to irradiation is described.

2.6 Waste management

After a nuclear power plant has reached their life-span decommissioning of the plant is necessary. Depending on the type of reactor irradiated graphite, worldwide do exist 250,000 tons, must be treated and disposed. However, not only the shutting down of nuclear power plants is a source for the increasing amount of irradiated graphite. But also the development in

the reactor designs. High temperature reactors (HTR) are graphite moderated [Gui 10], very high temperature reactors (VHTR) and pebble bed modular reactors (PBMR) use graphite encapsulated fuel particles for instance. Hence ways for disposing the waste are necessary.

To find the most appropriate solution the disadvantageous properties of irradiated graphite must be taken into account. The problems of irradiated graphite are the long half-life of C-14 (5730a), the characteristic that organisms can take it very easily up, the fact that up to 1% of irradiated graphite consist of C-14 and that it is combustible and vulnerable for oxidation whereas it is mostly inert. This leads to problems in the storage. Another critical point is the ability of graphite to store energy from neutrons in its structure in form of Wigner energy [Mcg 11].

Facing these problems from several ways of handling the graphite waste can be chosen. One way is the immobilization of graphite. One approach is discussed in [Mcg 11]. Sintering the activated graphite with glass is one suggestion. The glass composite material can then be used as structural or shielding material. This solution is for long-term disposal. It is an approach but no final route to dispose irradiated graphite.

Another way of immobilizing is described in [Pla 02]. There a cold hardening fixative is used for covering graphite from the RBMK masonry of a Leningrad nuclear power plant operated for 17 years. The fixative consists of epoxy oligomer, compacted with a furane heterocyclic alydehyde. The result is no release of radionuclides for 2 years at 20°C and for 1 year at 50°C.

In [Kar 05] an immobilizing treatment method is described to process reactor graphite waste into a matrix. For this a self sustaining exothermic reaction is used to produce a durable ceramic product Al_2O_3-TiC. The advantage is the good immobilization characteristic, which faces an increase in the waste volume.

Other suggestions are incineration and the direct disposal of the graphite. The first consideration is cheap but releases CO_2. The second approach is relatively expensive due to the building up of environmental barriers for the graphite and the costs for long time disposal sites.

The burning of irradiated graphite was also tried. In France it was tested at a low capacity experimental facility. The emission of CO_2 in the atmosphere (C-14), the strict requirements for the risk elimination and the huge amount of produced irradiated graphite are the developed problems of this disposal solution. Storage of the waste was seen as better alternative [Fro 04].

3 Autoradiography

The word “radiography” assembles out of the Latin prefix “radio” (=bar, beam) and the Greek word “graphein” (= to write). Under this word you understand the illustration of ionizing radiation with the help of photographic material. The resulting radiogram is created by the self-radiation of the measurement object or by activation [Neu 87]. Autoradiography developed due to the discovery of Niepce de Saint-Victor (1805-1870). In 1858 he found out, that a drawing made out of a special photo chemical (Uranylnitrat) can be copied to a photo plate. At present the autoradiography plays a role in quantitative, two-dimensional distributional analytical assays.

During time four radio-imaging-technologies were developed. The basic technique is the autoradiography via **film emulsion**. There, a radiogram on a film due to ionizing radiation is created with the help of a developer. The disadvantage of this method is the needed time to get a good picture of a sample with unknown activity. The possibility of analyzing uneven samples is an advantage. The **thin layer scanner** is another method of autoradiography. Here you put the probe on a table, adjustable in x- and y-direction, und a detector. A disadvantage is the limited sharpness of the sample image, as it must be a necessary distance between the probe and the detector. Changing something during the measurement is an advantage. Additionally there are radioimagers working with the principle of **solid state phosphorescence**. The image of the active sample is generated due to the fact that the recombined electrons, of the doted semiconductor atoms of the exposition material, emit photons. Disadvantage is the determination of the exposition time of probes with unknown activity. An advantage is the high resolution of the location.

Here the method of the **Instant-Imagers** is used. The characteristic of this method is the possibility to analyze the sample during the measurement. For the measurements here an Instant-Imager from the company Canberra Packard was used. He is built up of a detector, a power supply for the operation- and the high voltage and a PC inclusive a xy-decoder platin. The measurement principle of such an Instant-Imager-System is equal to a proportional counter tube. Approximately 210 000 proportional counter tubes are used in such an Instant-Imager.

These counter tubes correspond to bore holes of the diameter 0.4 mm with a pitch of 0.5 mm. The used gas consist of isobutan (1.0 Vol %), carbon dioxide (2.5 Vol %) and argon (96.5 Vol %). The plate (20x24) cm^2 with the bore holes is part of the so called **Mi**cro **c**hannel **a**rray **d**etector (MICAD). The MICAD consists of 11 layers of copper and fiber glass. Between these layers and the sample surface are lying different layers in the millimeter area. The purpose is the seal, as protection for contamination and to stabilize the detector mechanically. The task of the MICAD is the multiplication of the amount of electrons and the acceleration of the secondary electrons. The accelerated secondary electrons end up in the **M**ulti-**W**ire-**P**roportional-**C**ounter (MWPC). The MWPC is a cathode lattice made of copper stripes. The secondary electron out of the MICAD interacts with the HV-cathode level, so that an electrical impuls is detected and with the help of the channelboard in the Instant-Imager is the secondary electron a x-coordinate assigned. The secondary electron now flies through a focusing level, consisting out of 200 thin copper wires. After this the secondary electron ends up at another HV-level, which assigns the electron electronically a y-coordinate. Both coordinates are sent via seriel interfaces of the Instant-Imager in direction to the PC, where they are displayed on the screen [Vil 03].

4 Material and Methods

4.1 Graphite probes

Probe: Merlin1 out of the thermal column of the research reactor FRJ-1 (Merlin) (see figure 6 7 and table 2)

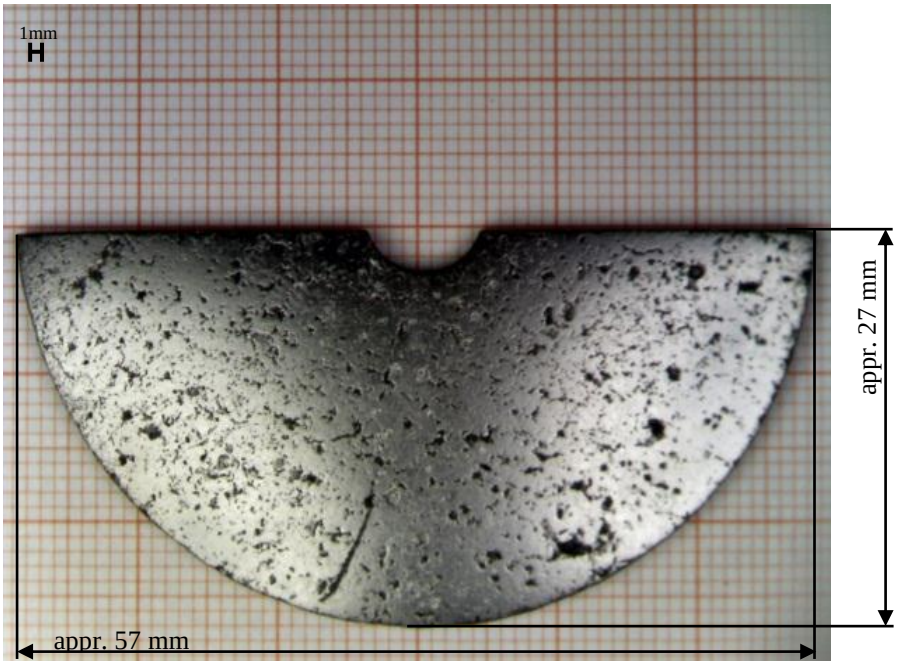

Figure 6: Merlin sample front

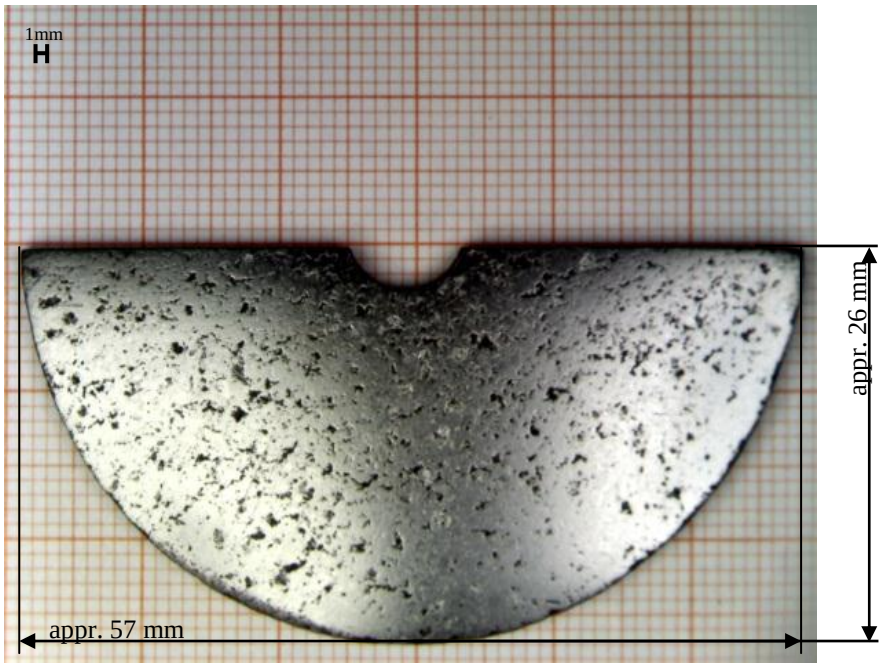

Figure 7: Merlin sample back

Quantity of graphite [te]: appr. 10 [Flo 09]

Purpose of the graphite: moderator (thermal column) [Flo 09], [Www 2]

Major Radionuclides: see table 2

Type of Reactor: research reactor [Flo 09]

Operation time: 1964 – 1985 [Flo 09]

Power Output (Th.): first: 5 MW, then 10 MW [Flo 09]

Table 2: Radionuclide Inventory of the Merlin sample.

Nuclide	Half-live [a]	Specific activity [Bq/g] 01.08.2008	Specific activity [Bq/g] 06.05.2011
H-3	12.33	3.54E+03	3.03E+03
C-14	5730	3.79E+02	3.79E+02
Fe-55	2.73	1.10E+02	5.46E+01
Co-60	5.271	3.32E+00	2.31E+00
Ba-133	10.54	1.03E+01	8.55E+00
Eu-152	13.3	5.29E+02	4.58E+02
Eu-154	8.8	2.97E+01	2.39E+01

Probe: St. Laurent A2 NPP (SLA), drilling probe of the height 5120 cm (see figure 8, 9 and table 3)

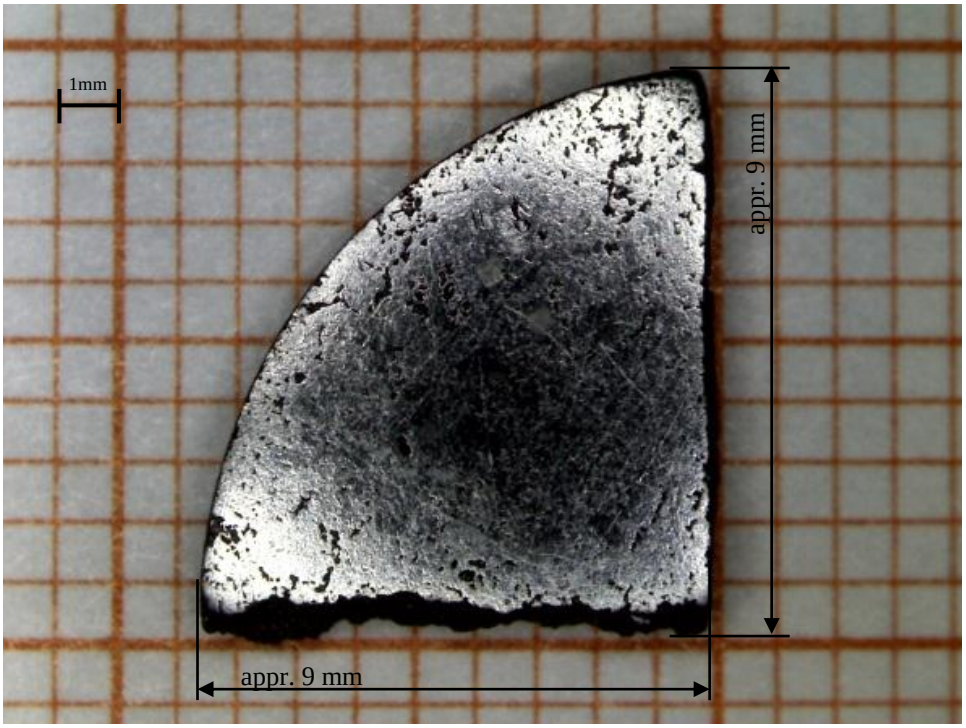

Figure 8: SLA sample; uneven side.

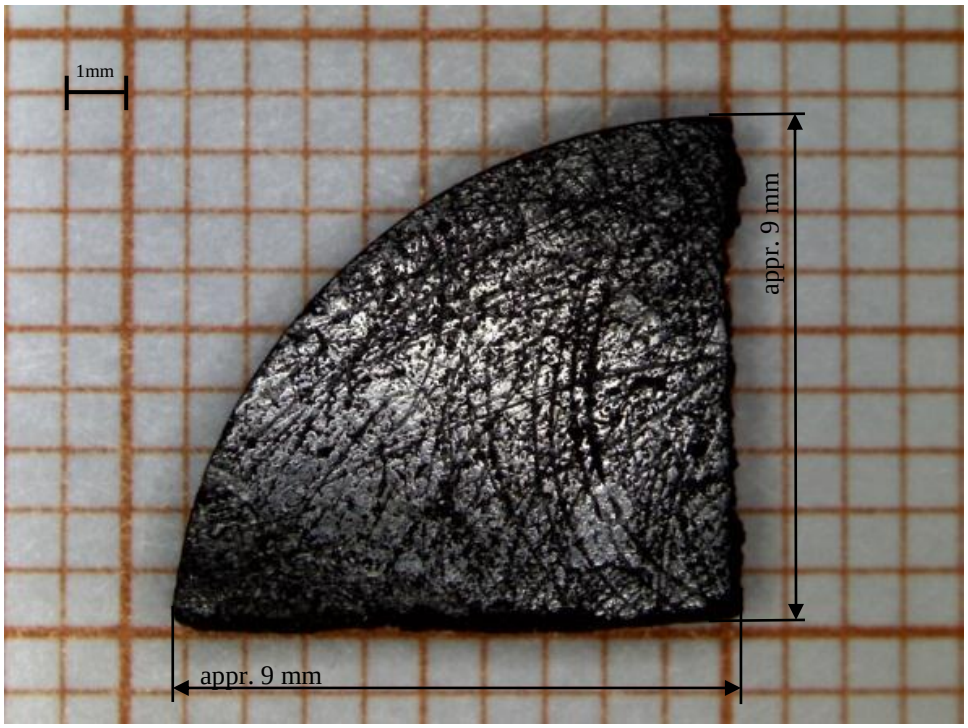

Figure 9: SLA sample; uneven side.

Quantity of graphite [te]: 3400 [Www 3]

Purpose of the graphite: moderator [Ia1 06]

Major Radionuclides: see table 3

Type of Reactor: energy production reactor / uranium natural graphite gas reactor (UNGG) [Www 3]

Operation time: 1971 – 1992 [Www 3]

Power Output (Th.): appr. 1260 [Www 3]

Table 3: Radionuclide Inventory of the SLA2-5120 sample.

Nuclide	Half-live [a]	Specific activity [Bq/g] 16.11.2010	Specific activity [Bq/g] 06.05.2011
H-3	12.33	3.48E+04	3.39E+04
C-14	5730	4.36E+04	4.36E+04
Co-60	5.271	3.62E+04	3.4E+04
Cs-134	2.1	1.28E+01	1.10E+01
Cs-137	30.2	6.99E+01	6.92E+01
Ba-133	10.54	9.19E+01	8.91E+01
Eu-154	8.8	1.56E+02	1.50E+02
Eu-155	4.8	4.60E+01	4.30E+01

Probe: DIDO scretch sample out of the 6VGR-chanel of the graphite reflector

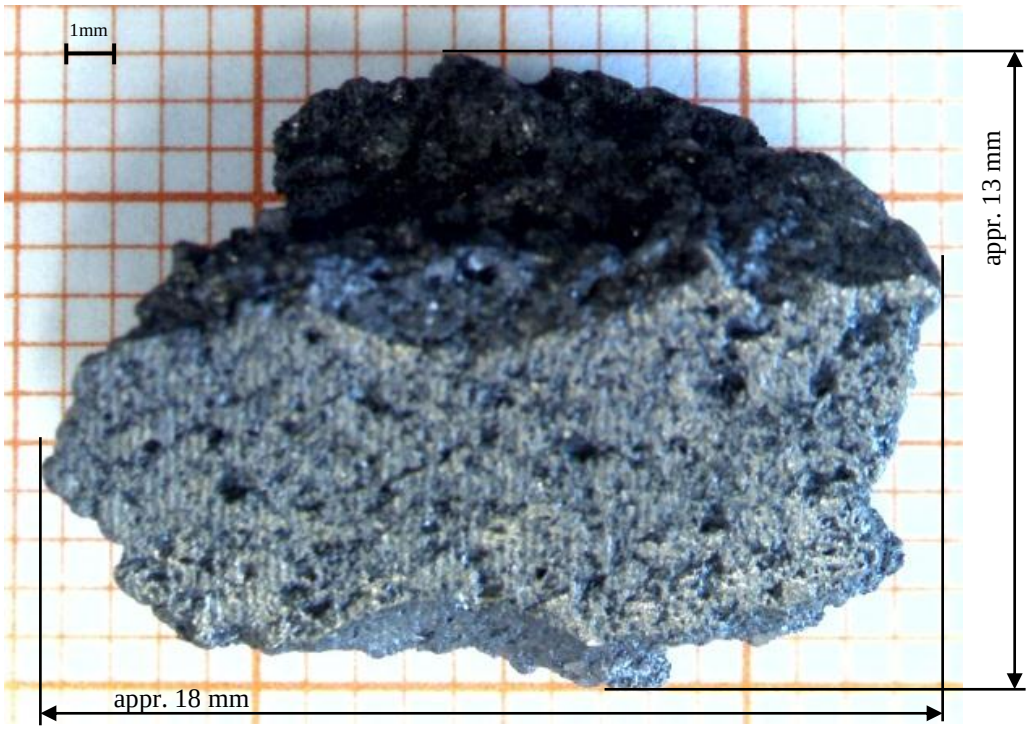

Figure 10: Even side of the DIDO sample.

Figure 11: Uneven side of the DIDO sample.

Quantity of graphite [te]: 17 [Wis 06]

Purpose of the graphite: only reflector [Wis 06]

Major Radionuclides: H-3, C-14 [Wis 06]

Type of Reactor: Research Reactor – Material testing reactor [Wis 06]

Operation time: 1956 – 1990 [Wis 06]

Power Output (Th.): 10-26 MW [Wis 06]

Table 4: Radionuclide Inventory of the DIDO sample.

Radionuclide	Half-life [a]	Specific activity [Bq/g] 01.02.2010	Specific activity [Bq/g] 04.07.2011
H-3	12.33	2.6E+06	2.4E+06
C-14	5730	9.8E+04	9.8E+04
Fe-55	2,73	9.7E+03	6.8E+03
Co-60	5.271	8.9E+03	7.4E+03
Cs-134	2.1	4.3E+02	2.7E+02
Cs-137	30.2	7.7E+01	7.5E+01
Ba-133	10.54	2.0E+02	1.8E+02
Eu-154	8.8	2.6E+03	2.3E+03
Eu-155	4.8	1.6E+03	1.3E+03

Probe: RBMK sample out of a fuel channel of the NPP Ignalina I (see figure 12, 13 and table 5)

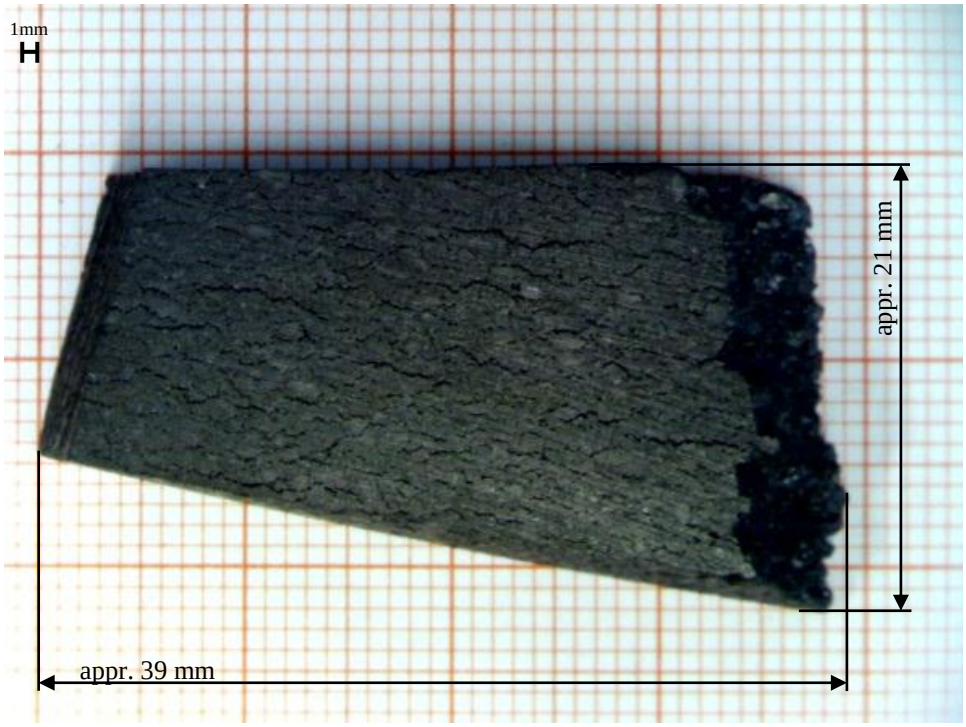

Figure 12: Side A of the RBMK sample.

Figure 13: Side B of the RBMK sample.

Quantity of graphite [te]: 1921.5 [Puz 10]

Purpose of the graphite: moderator and reflector [Ned 11], [Anc 05]

Major Radionuclides: see table 5

Type of Reactor: energy production reactor / RBMK-1500 [Ned 11]

Operation time: 1983 – 2004 [Ned 11]

Power Output (Th.): 4800 MW [Ia2 04]

Table 5: Radionuclide inventory of the RBMK sample.

Radionuclide	Half-life [a]	Specific activity [Bq/g] 11.07.2009	Specific activity [Bq/g] 04.07.2011
C-14	5730	2.4E+04	2.4E+04
Mn-54	0.855	9.9E+00	2.0E+00
Co-60	5.271	4.0E+01	3.1E+01
Cs-137	30.2	7.0E-01	6.7E-01

Probe: AVR (Arbeitsgemeinschaft Versuchsreaktor) sample is a flaking of the inner graphite-built ins (see figure 14, 15 and table 6)

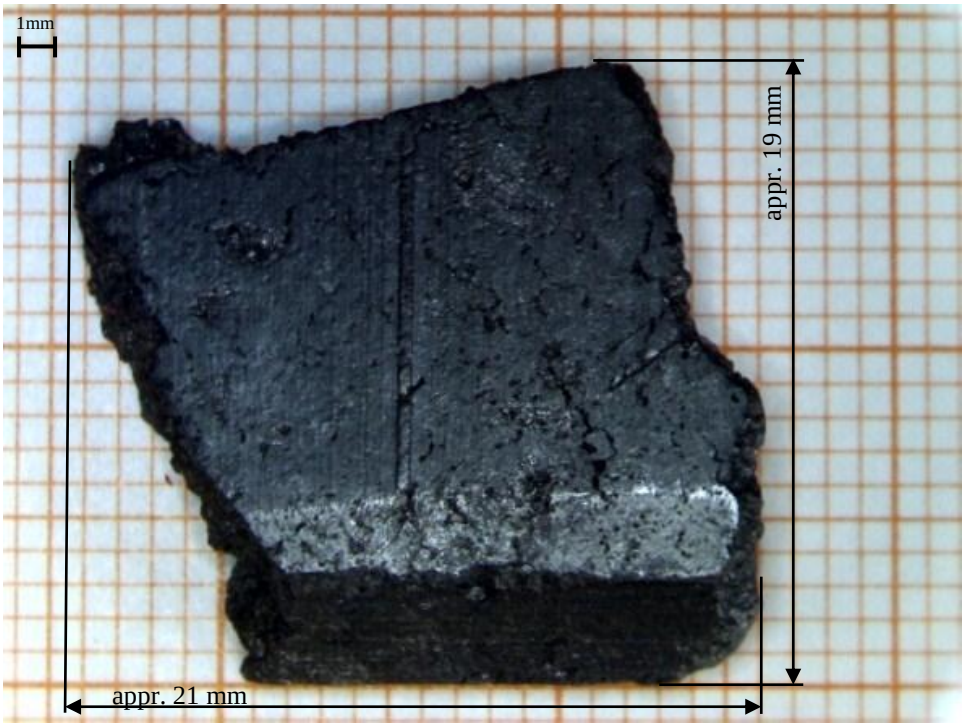

Figure 14: Even side of the AVR sample.

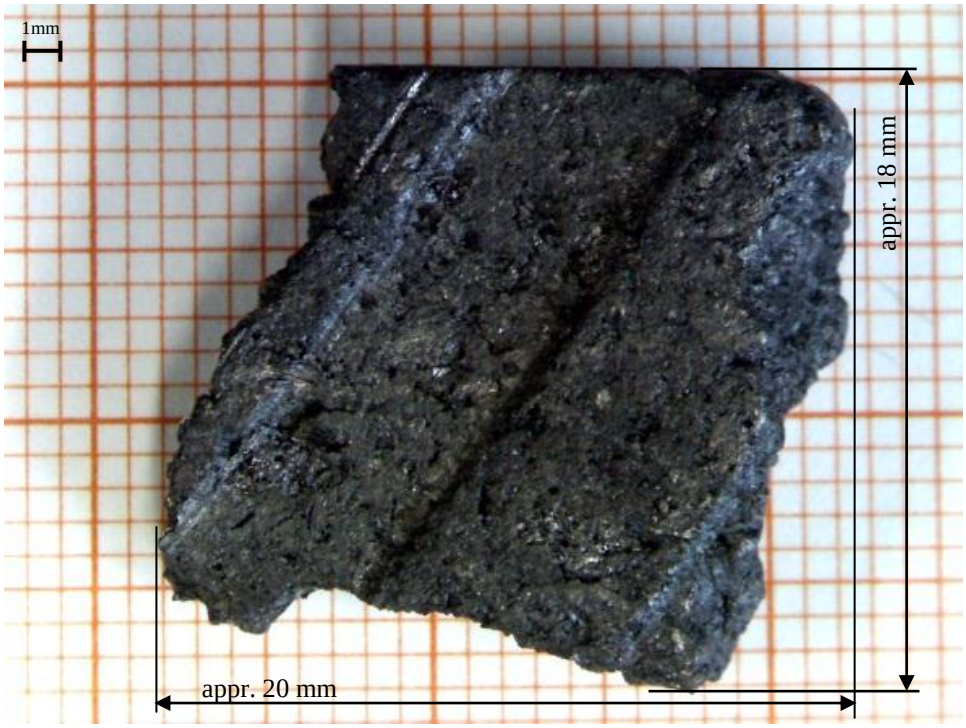

Figure 15: Uneven side of the AVR sample.

Quantity of graphite [te]: 67 (graphite-built ins) + 158 (carbon bricks built-in)

Purpose of the graphite: as basic material for core structures (high-purity graphite), as insulation layer for the graphite reflector (more impurities), moderator [Bis 01]

Major Radionuclides: see table 6

Type of Reactor: experimental reactor [Bis 01]

Operation time: 1968 – 1988 [Bis 01]

Power Output (Th.): appr. 45 MW [Bis 01]

Table 6: Nuclide inventory of the AVR sample.

Radionuclide	Half-life [a]	Specific activity [Bq/g] 01.10.2007	Specific activity [Bq/g] 04.07.2011
H-3	12.33	1.0E+07	8.3E+06
C-14	5730	3.3E+05	3.3E+05
Fe-55	2,73	6.8E+03	2.6E+03
Co-60	5.271	1.2E+04	7.1E+03
Sr-90	28.5	2.5E+05	2.3E+05
Cs-134	2.1	1.3E+02	3.6E+01
Cs-137	30.2	2.3E+04	2.1E+04
Ba-133	10.54	6.8E+02	5.3E+02
Eu-154	8.8	2.2E+02	1.7E+02
Eu-155	4.8	9.0E+01	5.3E+01

4.2 Absorption measurements

Before starting with the autoradiographic measurements absorption curves were empirically taken. The measurements had the aim to verify the already known theoretical absorption behavior of several radioactive elements regarding the absorption with aluminum. The results made it possible calculating the necessary absorption thicknesses for the measurements with the Instant-Imager.

4.2.1 Sources

The used sources for making the absorption curves are shown in figure 16, 17, 18 and 19.

Cs-137

Figure 16: Selfmade Cs-137 source; Diameter: 2.9 cm; Activity unknown

Sr-90

Figure 17: Big opening (Diameter: 3-4 mm), 8 µCi (23.04.1981)

Co-60

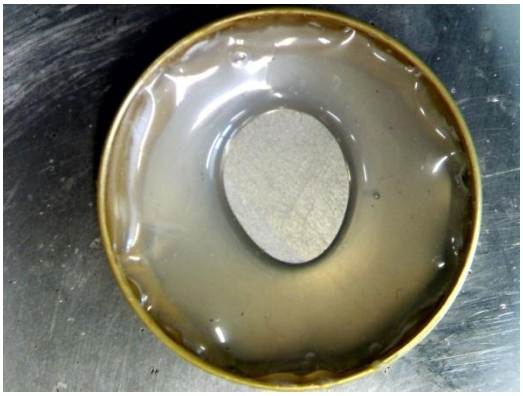

Figure 18: Selfmade Co-60 source; diameter: 2.90 cm; activity: 2 kBq

Cl-36

A point source was used

4.2.2 Absorber

Two kinds of filter set were used. The filters of both sets consisted of aluminum. One filter set (serial No.: s6819) was from the company Picker nuclear. It consisted out of ten different filters. The other set (605/x) contains 30 filters of different thickness. Figure 19 gives an impression of this types of filter.

Figure 19: Used filtersets for measuring the absorption curves. On the left the set with 30 filters. On the right the set from Pickers with 10 filters.

4.2.3 Detector and Serial Micro Channel SMC 2100

The Serial Micro Channel SMC 2100 is the interface between the GM-Counter and the measurement software. It is a product of the company FST Freiberger Sensortechnik GbR (Freiberg/Saxony). Figure 21 gives an impression of this electronic device [Han 00].

Figure 21: Measurement stand for receiving the absorption curves. Left: PC with measurement software; Middle: SMC device; Right: Geiger-Müller Counter

The detector, from LND INC.(USA), is connected via a coaxial cable to the device. Via RS232-interface the electronic signals are sent to the analyzing software. Figure 22 shows the user interface of the software for a start-stop measurement.

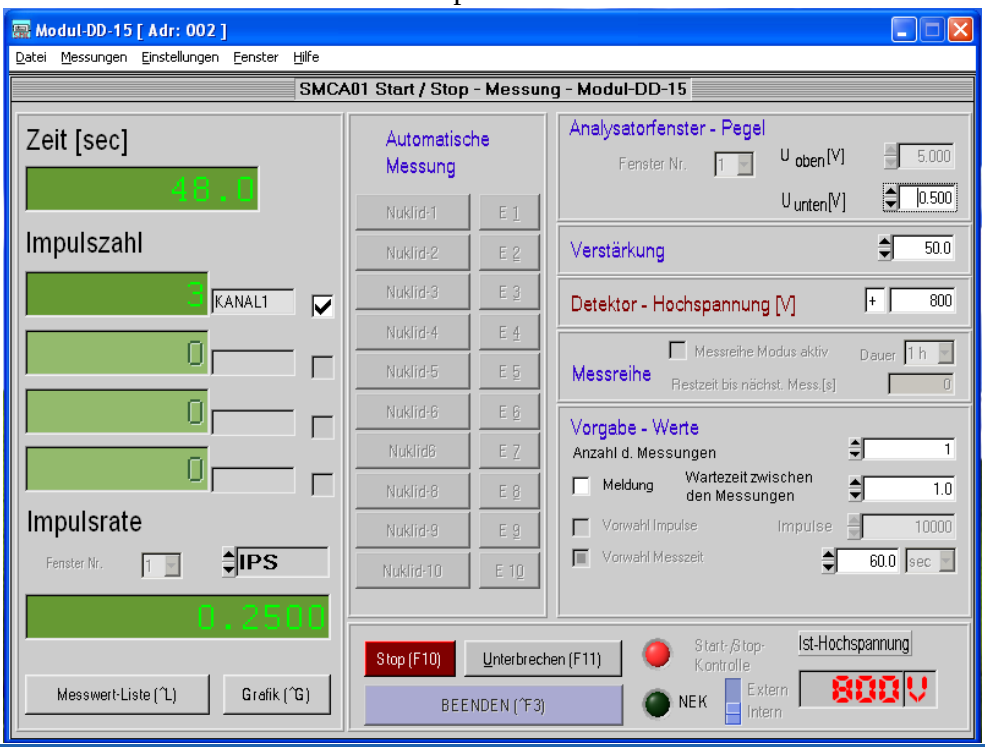

Figure 22: Screenshot of the used software for detecting the radioactivity of sources.

4.3 Aluminum absorbers

The results (half-thickness) of the empirically gained absorption curves where used to calculate the thickness of the aluminum absorbers for the measurements with the Instant-Imager. In table 7 the multiples of the half-thickness for Aluminum, which are then used for realizing the absorbers, are shown.

Table 7: Calculated values for the half-thickness to realize the aluminum absorbers for the Instant-Imager measurements.

Nuclide	E(γ) [keV]	I(γ) [%]	E(β max) [keV]	I(β) [%]	HWD [mg/cm2]	HWD Alu [mm]	3 HWD [mm]	7 HWD [mm]
						2700		
^{3}H			18.591	100				
^{14}C			156.475	100	2.9	0.0107	0.0322	0.0751
^{36}Cl			709.23	98.1	29	0.1074	0.3222	0.7518
^{60}Co	1173.237 1332.501	99.9736 99.9856	318.13	99.925	8.4	0.0311	0.0933	0.2177
^{137}Cs	661.657	85.1	513.97	94.4	17.5	0.0648	0.1944	0.4537
^{90}Sr			0.546		19.5	0.0722	0.2166	0.5055
^{90}Y			2.27		165	0.6111	1.8333	4.2777

The received values for half-thickness (three/seven times) were gathered in six groups shown in table 8. Whereas each group value stands for the thickness (in cm) of the used aluminum absorber in the Instant-Imager measurements.

Table 8: Finding the values for the aluminum absorbers.

Received values for half-thickness [mm]	Group value [mm] = thickness of aluminum absorbers [mm]
0.0322, 0.0752, 0.0933	0.1
0.2055 (mean of 0.19 and 0.21), 0.2178	0.225
0.3222	0.3
0.4796	0.5
0.7519	0.725
1.8333, 4.2778	4.3

4.4 Measurements with the Instant-Imager

4.4.1 Absorber

The material for the absorbers comes from the company Goodfellow Cambridge Limited (Huntingdon, England) and from Alfa Aesar® (A Johnson Matthey Company) (Karlsruhe, Germany). The constituents of each absorber are shown in table 9.

Table 9: Building up of the final absorber thickness.

Final absorber thickness [mm]	Separate elements
4.3	(2 x 1 mm) + (1 x 2.3 mm)
0.725	(2 x 0.2 mm) + (1 X 0.1 mm) + (1 x 0.125 mm)
0.5	(2 x 0.2 mm) + (1 X 0.1 mm)
0.3	(1 x 0.1 mm) + (1 x 0.2 mm)
0.225	(1 x 0.1 mm) + (1 x 0.125 mm)
0.1	1 x 0.1 mm

The properties of each aluminum part are described now.

Aluminum foil – 0.1 mm

Company: Goodfellow

Thickness [mm]: 0.1

Purity [%]: 99.0

degree of hardness: annealed

Aluminum foil – 0.125 mm

Company: Goodfellow

Thickness [mm]: 0.125

Purity [%]: 99.0

degree of hardness: annealed

Aluminum foil – 0.2 mm

Company: Goodfellow

Thickness [mm]: 0.2

Purity [%]: 99.0

degree of hardness: annealed

Aluminum foil – 1.0 mm

Company: Alfa Aesar

Thickness [mm]: 1.0

Alloy 6061

Aluminum foil – 2.3 mm

Company: Alfa Aesar

Thickness [mm]: 2.3

5 Results

5.1 Absorption curves

Absorption curves were taken to verify the theory regarding half-thickness. The received information (half-thickness) made it possible to realize the aluminum absorbers for the Instant-Imager measurements.

5.1.1 Cl-36

The fitting function

$$R = R_{0,\beta^-} \cdot e^{-\left(\frac{ln2}{half-thickness,\beta^-} \cdot area\,density\right)} + constant$$

With

R_{0,β^-} = count rate for area density zero

Half-thickness = half-thickness of aluminum for the β^--energy

Area density = area density of the absorbers

in combination with the usage of the analyzing program Solver of Excel lead to the value for the half-thickness (300 g/m²).

The following figure shows the characteristics of the count rate dependent from the area density of the aluminum absorbers.

The parameters of the fitting equation

R_{0,β^-} = 172 cps half-thickness = 300 g/m² constant = 0.46

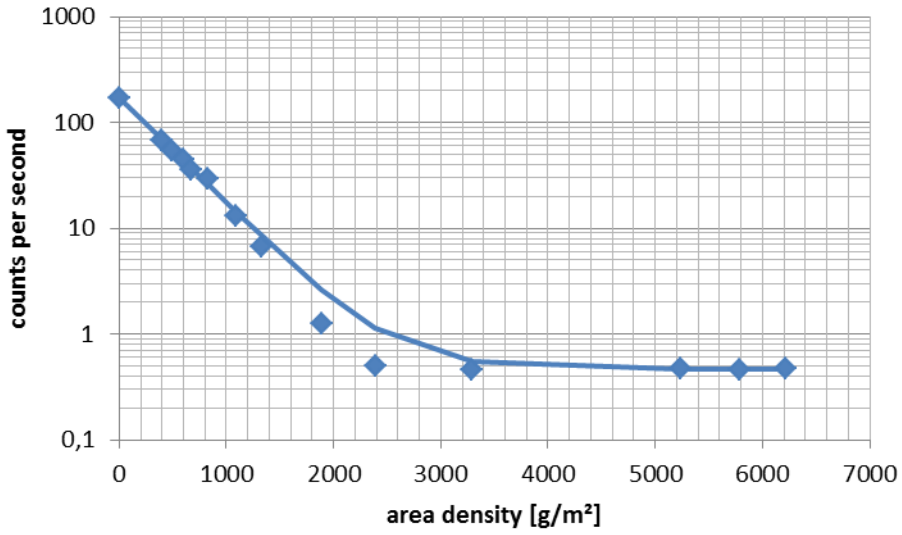

Figure 21: Absorption curve of Cl-36.

5.1.2 Cs-137

The fitting equation for Cs-137 consists of two parts. The reason is the β^- – and the γ-emission.

The fitting equation

$$R = R_{0,\beta^-} \cdot e^{-\left(\frac{ln2}{half-thickness,\beta^-} \cdot area\ density\right)} + R_{0,\gamma} \cdot e^{-\left(\frac{ln2}{half-thickness,\gamma} \cdot area\ density\right)}$$

results in following fitting parameters.

R_{0,β^-} = 1201 cps, $half - thickness,\beta^-$ = 230 g/m²

$R_{0,\gamma}$ = 23 cps $half - thickness,\gamma$ = 40 000 g/m²

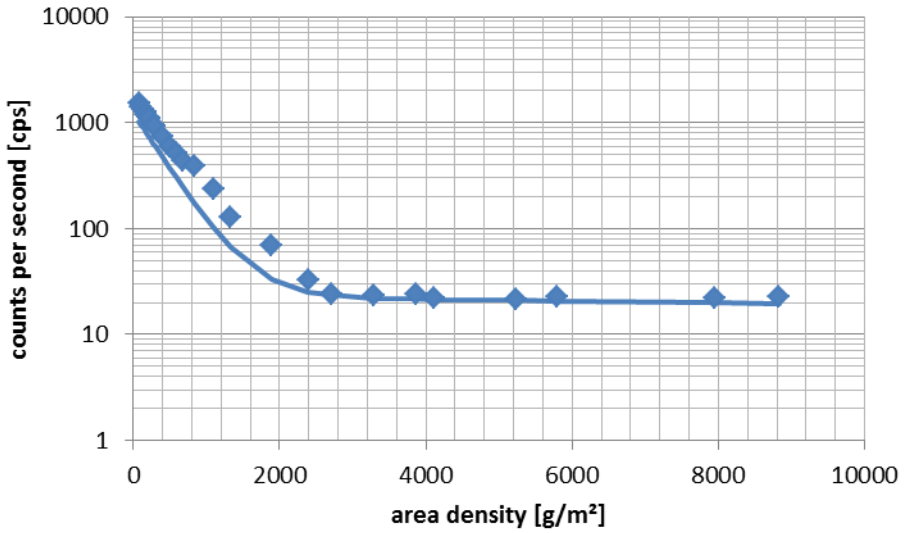

Figure 22: Absorption curve of Cs-137.

5.1.3 Sr-90 / Y-90

The fitting equation for this radionuclide equals the one for Cl-36 as the radiation has just a β^--part.

$R_{0,\beta-} = 1023\ cps$ half-thickness = 1023 g/m² constant = 1.5

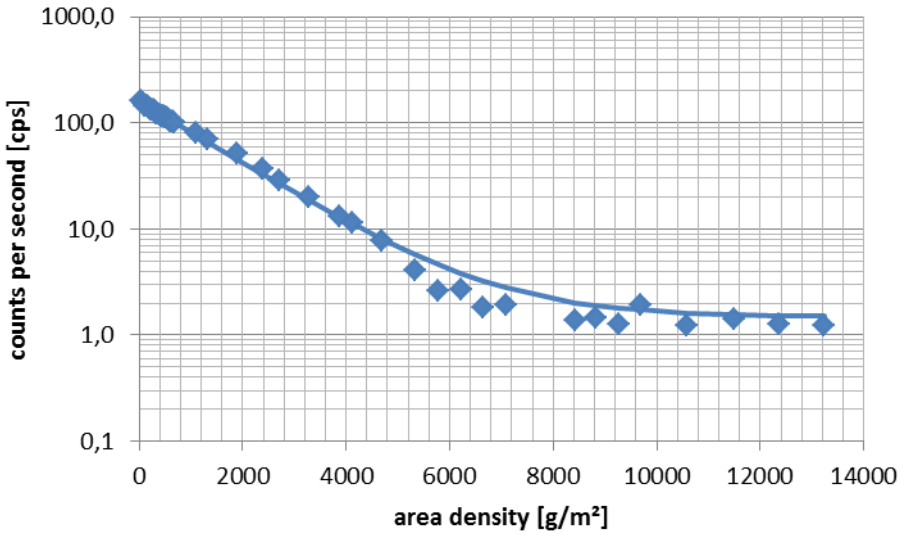

Figure 23: Absorption curve of Sr-90.

5.1.4 Co-60

Selfmade source

Co-60 has both a β^-- and a γ-part. Therefore the fitting equation is like the one for Cs-137. The fitting parameters are

R_{0,β^-} = 73 cps

$half-thickness,\beta^- = 186\ 914$ g/m²

$R_{0,\gamma} = 707\ cps$

$half-thickness,\gamma = 82$ g/m²

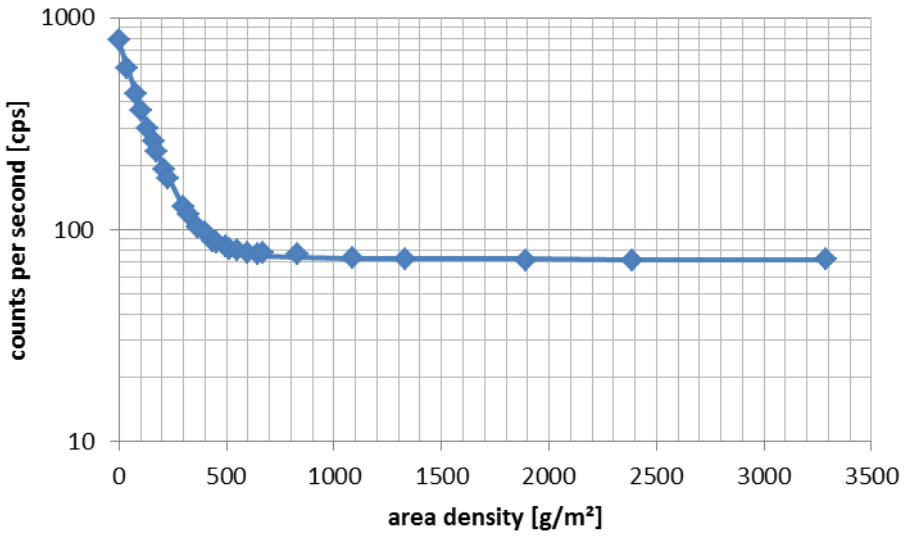

Figure 24: Absorption curve of Co-60 (selfmade source).

Point source

R_{0,β^-} = 18 cps $\quad half-thickness,\beta^- = 519$ g/m²

$R_{0,\gamma}$ = 35 cps $\quad half-thickness,\gamma = 89900$ g/m²

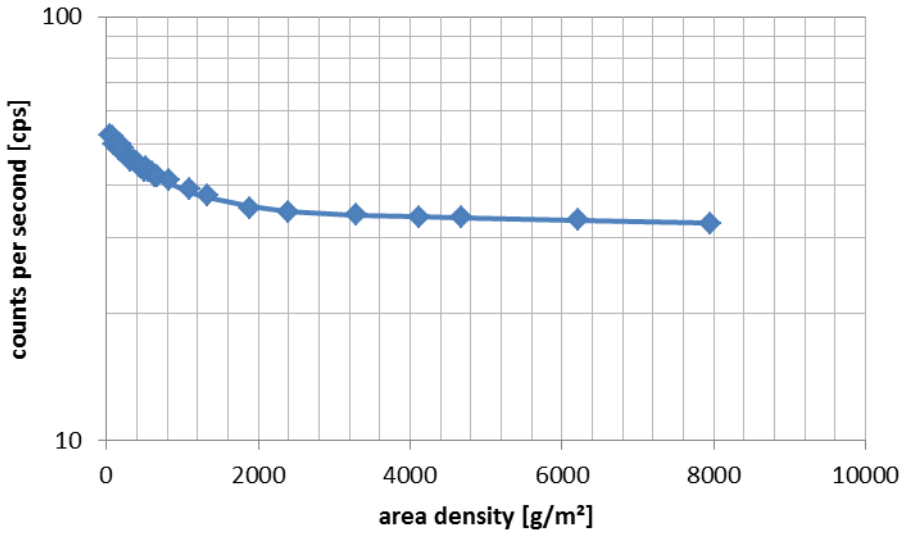

Figure 25: Absorption curve of Co-60 (point source).

5.2 Measurements with the Instant-Imager

In Figure 26 the Instant-Imager is shown.

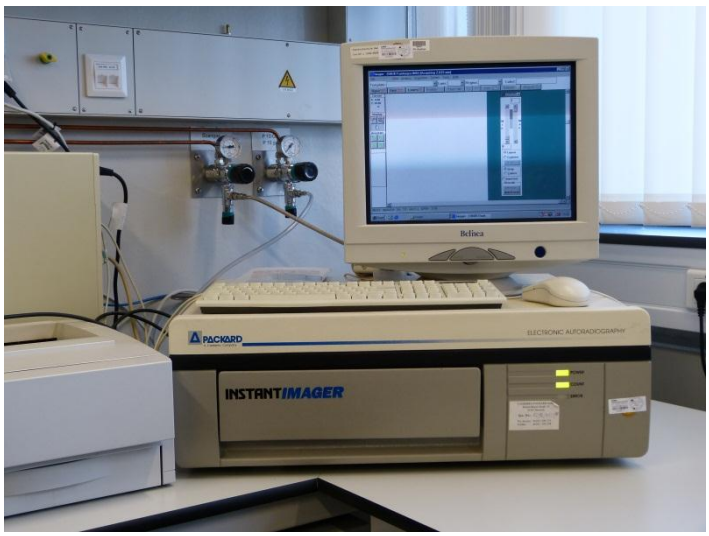

Figure 26: Instant-Imager

With the help of the absorbers in Figure 27 all the graphite samples were measured. In the left picture you can see the above surface of the absorbers. In the right picture the down side is displayed. The absorber A has the thickness 4.3 mm (on the left). In the middle (B) is the absorber located with the thickness of 0.5 mm (on the left) and 0.725 mm (on the right). The absorber down (C) has on the left the thickness of 0.1 mm, in the middle 0.225 mm and on the right 0.3 mm.

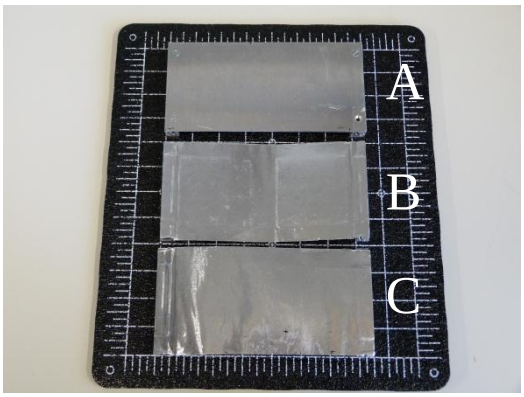

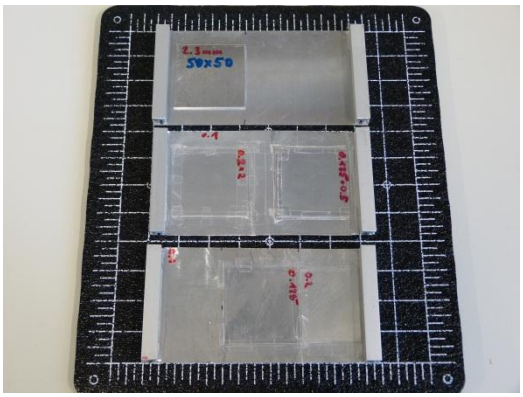

Figure 27: Used aluminum absorbers .

Figure 27 shows the used absorbers. Above them the masks, in which the absorbers have been laid to bring them in a defined position in the Instant-Imager. Reducing the distance between the surface of the graphite sample and the surface of the aluminum absorber the staples of paper, above the masks, are used. The rectangle above the masks is used to bring the sample-mask-composition in a defined position in the Instant-Imager.

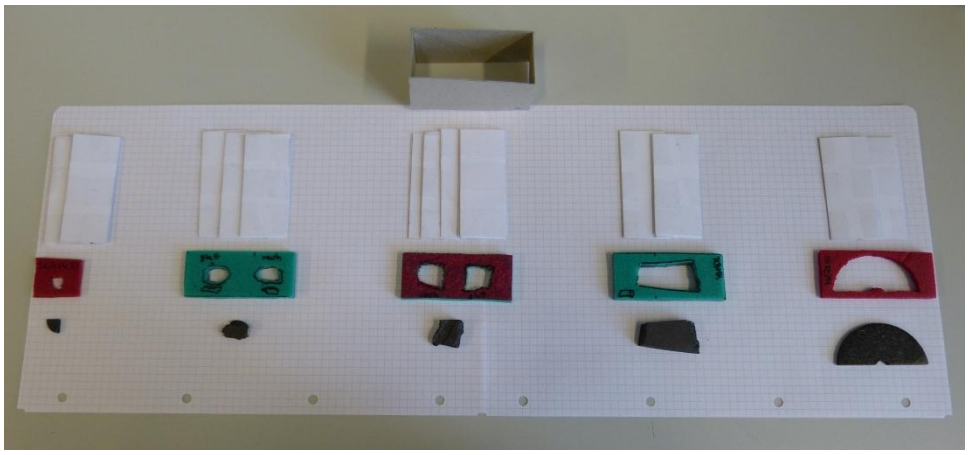

Figure 28: A: Graphite samples with its masks and paper staples. Above the paper rectangle.

Figure 29 shows the order for the several components (paper staple, mask, graphite sample and absorber) for a normal measurement.

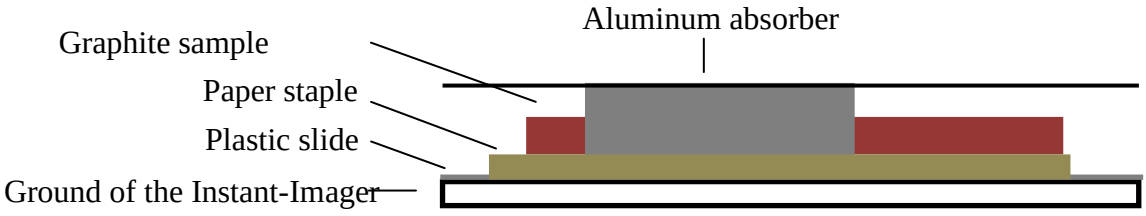

Figure 29: Assembly of the components for a measurement.

Explanation of the file names

SLA2

1_s3_we

1 = just for generating an order

s = stands for SLA

3 = third measurement

w = **w**ithout absorber

e = **e**ven side up / un = **un**even side up

2_s3_1e

1 = absorber thickness 0.**1** mm

2 = absorber thickness 0.225 mm

3= absorber thickness 0.3 mm

5 = absorber thickness 0.5 mm

7 = absorber thickness 0.725 mm

4 = absorber thickness 4.3 mm

Diff_SLA_e_wm1_ri_nT

Diff = **diff**erence of two instant imager pictures

SLA or S = stands for the name of the sample

e = **e**ven side up / un = **un**even side up

wm1 = image **w**ithout absorber **m**inus image with absorber of thickness 0.**1** mm

ri = **r**esult **i**nverted (= the resulting image out of the subtraction was inverted in the program ImageJ)

nT = **n**o **T**ranslation (of the images before the subtraction in ImageJ)

T = **T**ranslation (the image without absorber was defined as reference. Hence the image taken with the absorber was translated)

All mentioned abbreviations are also valid for the other samples. Following sample specific abbreviations are explained.

DIDO

D = stands for DIDO

AVR

A, a = stands for AVR

RBMK

R = stands for RBMK

s = slope side up

f = flat side up

MERLIN

M = stands for MERLIN

vlu = vertical line up

vld = vertical line down

5.2.1 Saint Laurent A2

5.2.1.1 Even side up

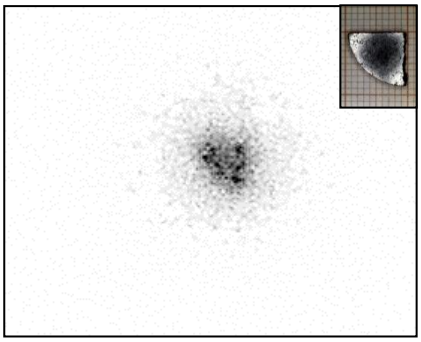

File: 1_s3_we

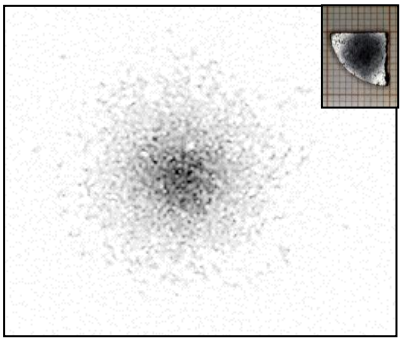

File: 2_s3_1e

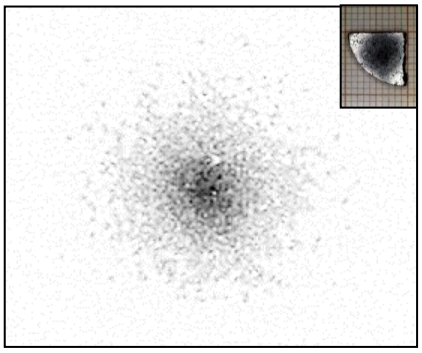

File: 3_s3_2e

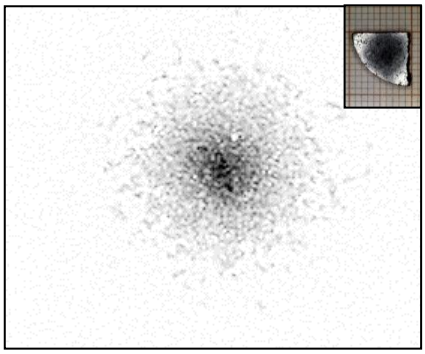

File: 4_s3_3e

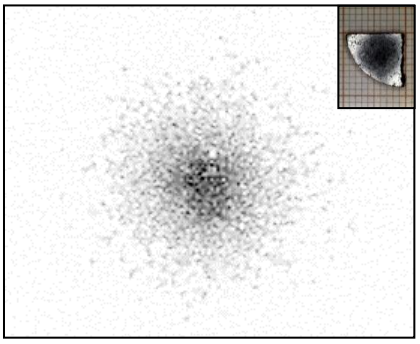

File: 5_s3_5e

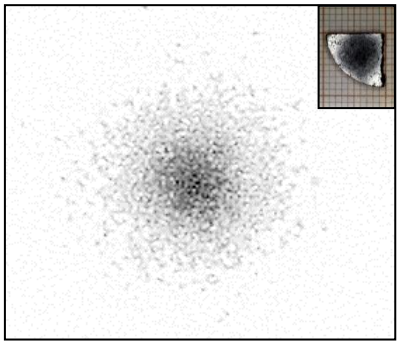

File: 6_s3_7e

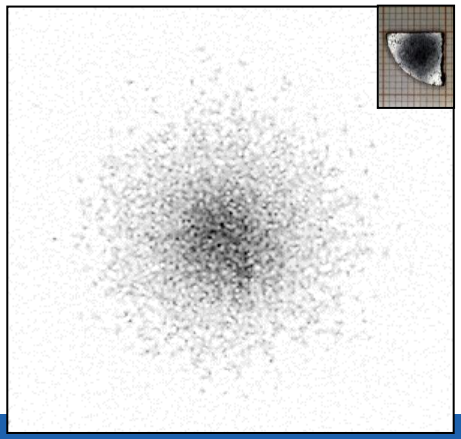

File: 7_s3_4e

5.2.1.2 Uneven side up

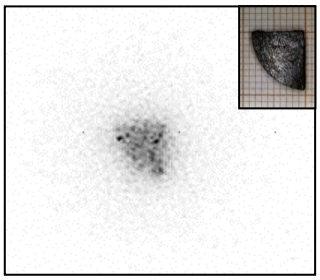

File: 1_s3_wun

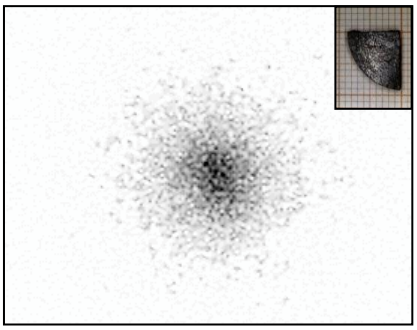

File: 2_s3_1un

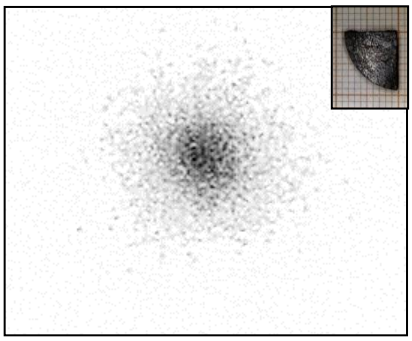

File: 3_s3_2un

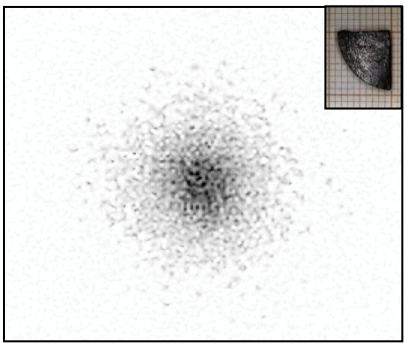

File: 4_s3_3un

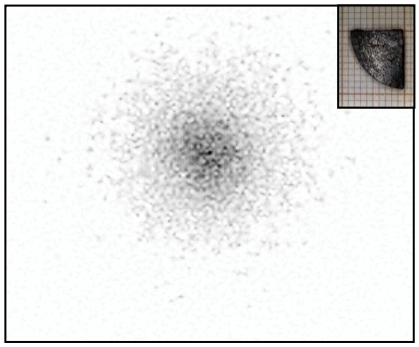

File: 5_s3_5un

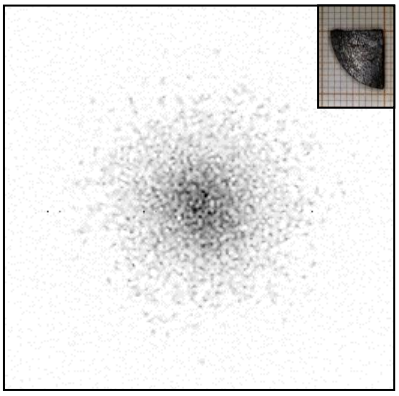

File: 6_s3_7un

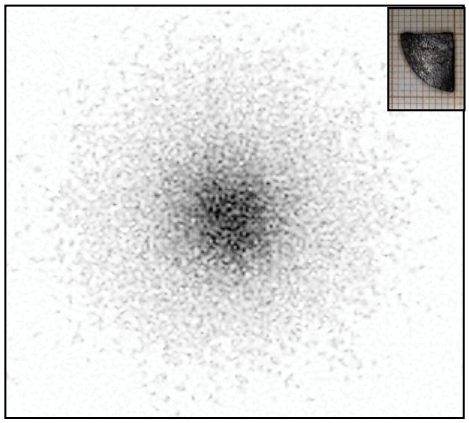

File: 7_s3_4un

5.2.1.3 Subtraction – Even side up [not translated + inverted images]

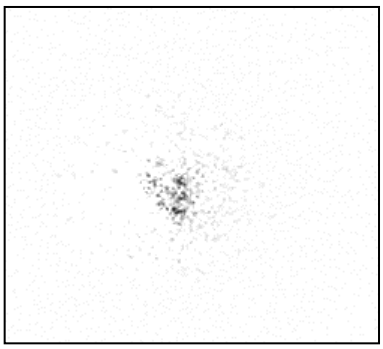

File: Diff_SLA_e_wm1_ri_nT

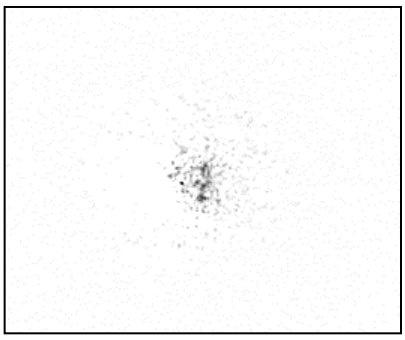

File: Diff_SLA_e_wm2_ri_nT

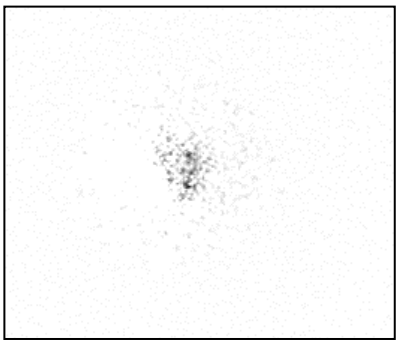

File: Diff_SLA_e_wm3_ri_nT

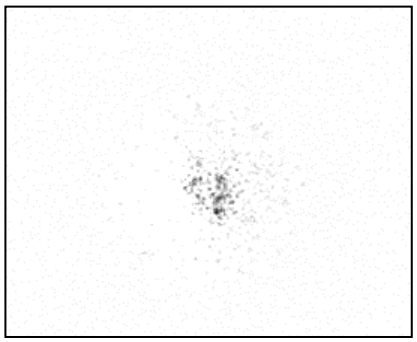

File: Diff_SLA_e_wm5_ri_nT

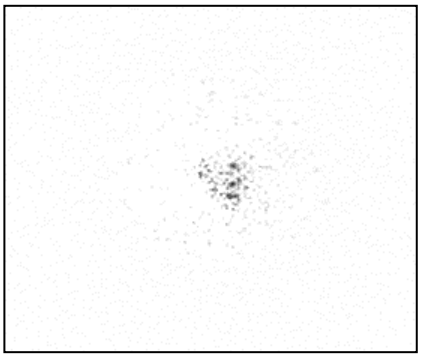

File: Diff_SLA_e_wm7_ri_nT

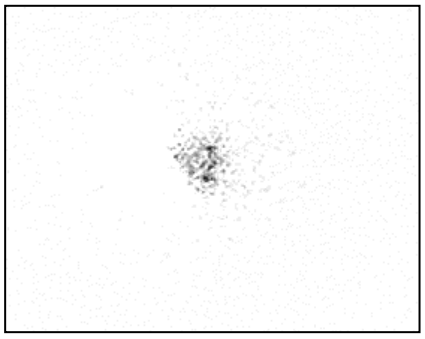

File: Diff_SLA_e_wm4_ri_nT

5.2.1.4 Subtraction – Even side up [translated + inverted images]

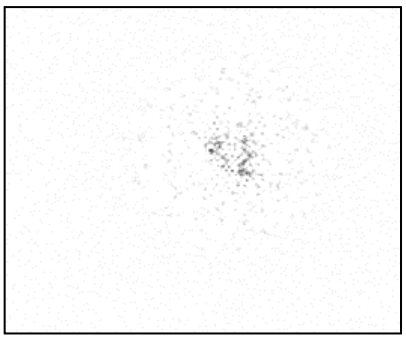

File: Diff_S_e_wm1_ri_T

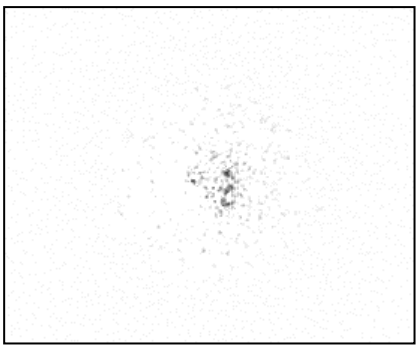

File: Diff_S_e_wm2_ri_T

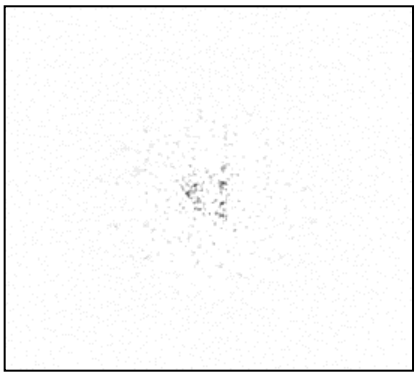

File: Diff_S_e_wm3_ri_T

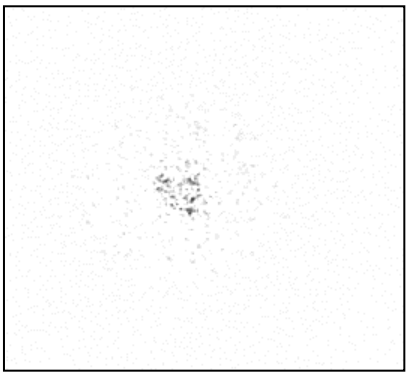

File: Diff_S_e_wm5_ri_T

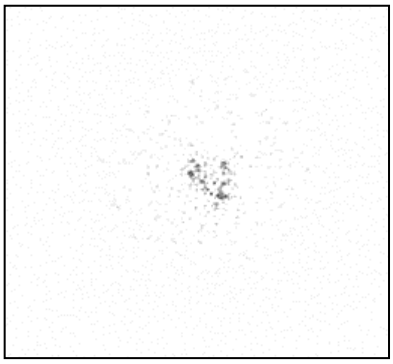

File: Diff_S_e_wm7_ri_T

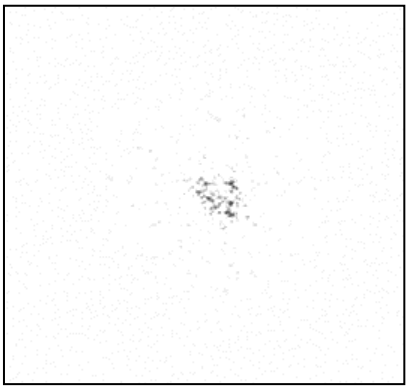

File: Diff_S_e_wm4_ri_T

5.2.1.5 Subtraction – Uneven side up [not translated + inverted images]

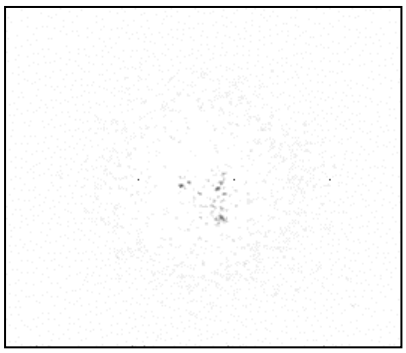

File: Diff_SLA_un_wm1_ri

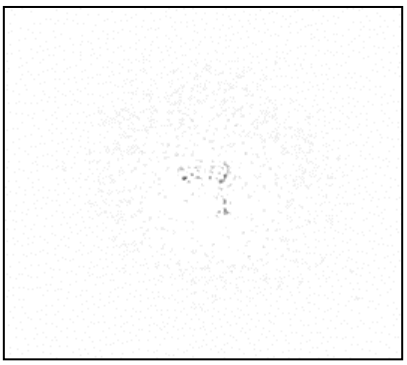

File: Diff_SLA_un_wm2_ri

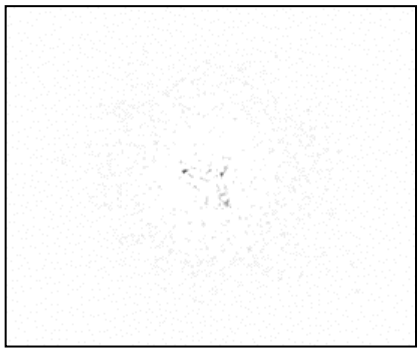

File: Diff_SLA_un_wm3_ri

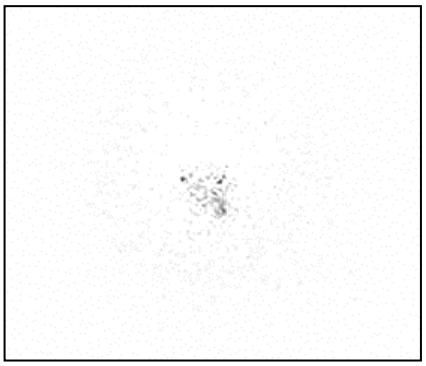

File: Diff_SLA_un_wm5_ri

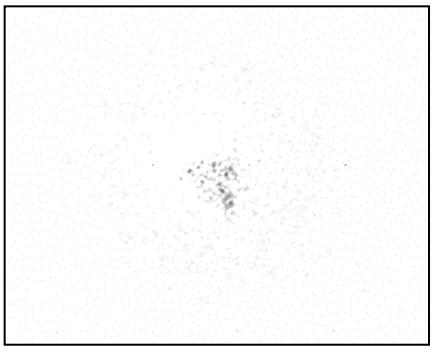

File: Diff_SLA_un_wm7_ri

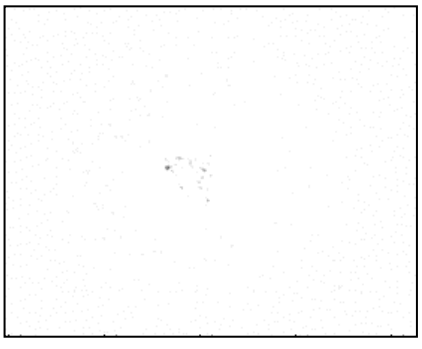

File: Diff_SLA_un_wm4_ri

5.2.1.6 Subtraction – Uneven side up [translated + inverted images]

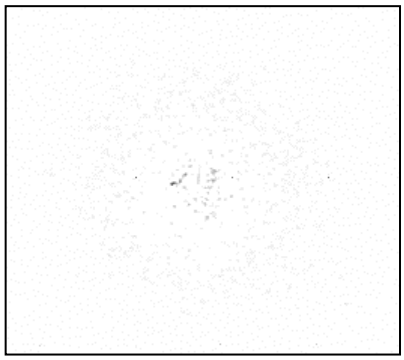

File: Diff_S_un_wm1_ri_T

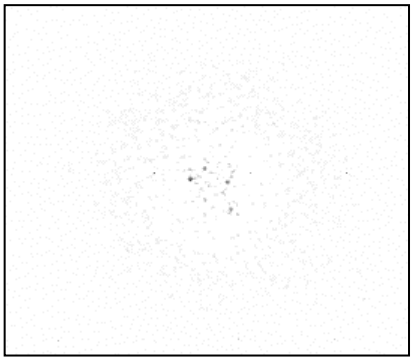

File: Diff_S_un_wm3_ri_T

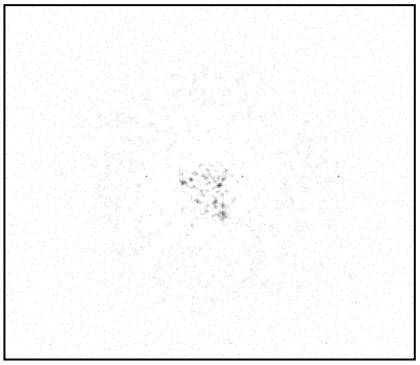

File: Diff_S_un_wm5_ri_T

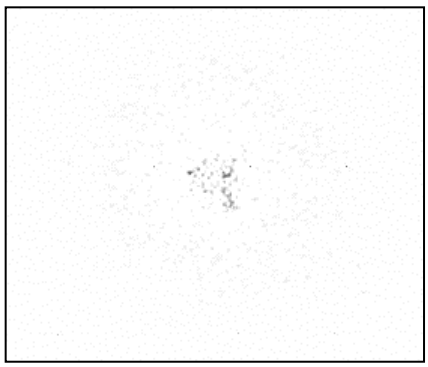

File: Diff_S_un_wm7_ri_T

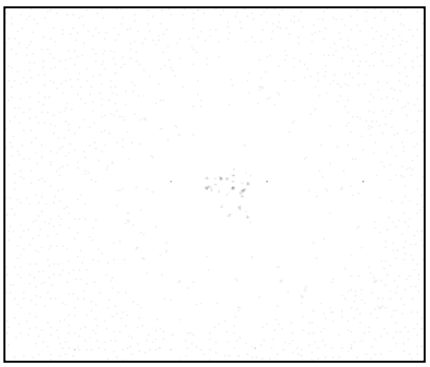

File: Diff_S_un_wm4_ri_T

5.2.2 DIDO

5.2.2.1 Even side up

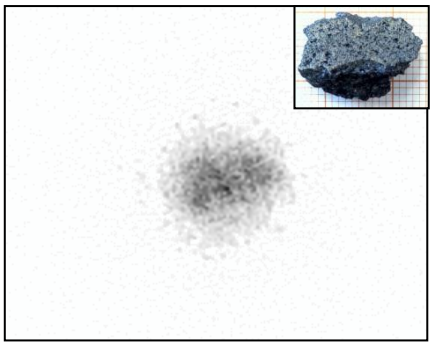

File: d3_we

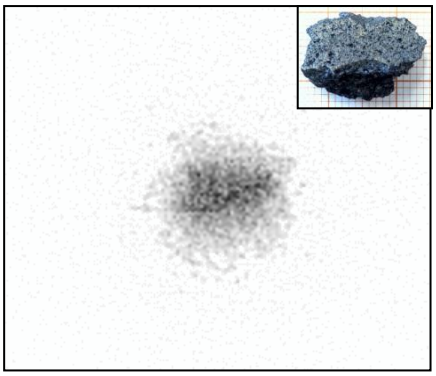

File: d3_1e

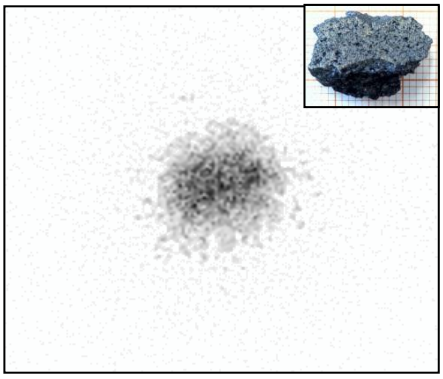

File: d3_2e

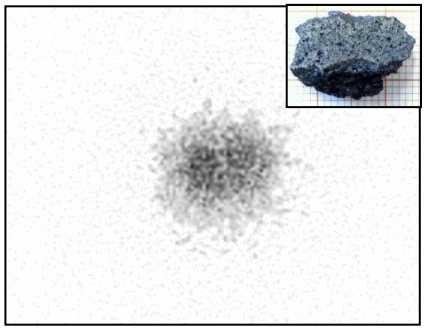

File: d3_3e

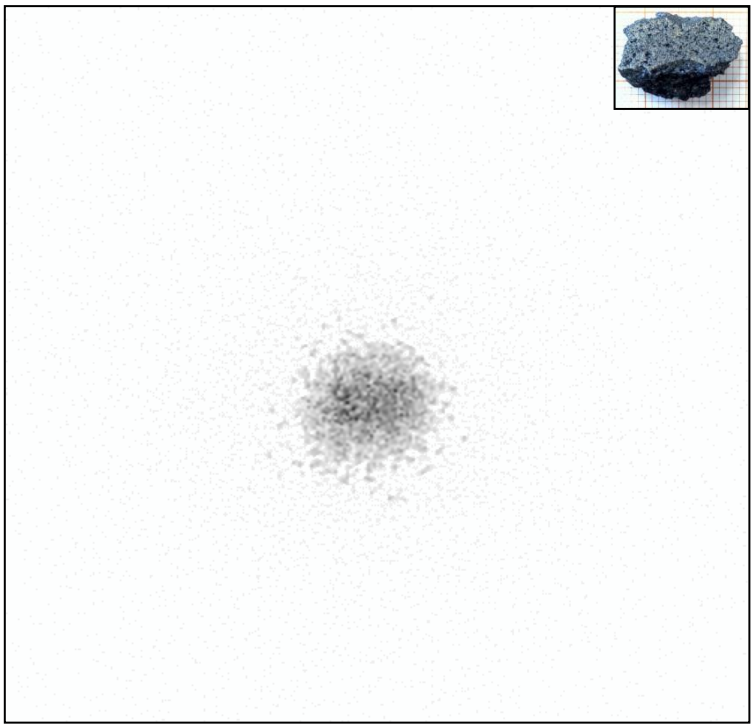

File: d3_5e

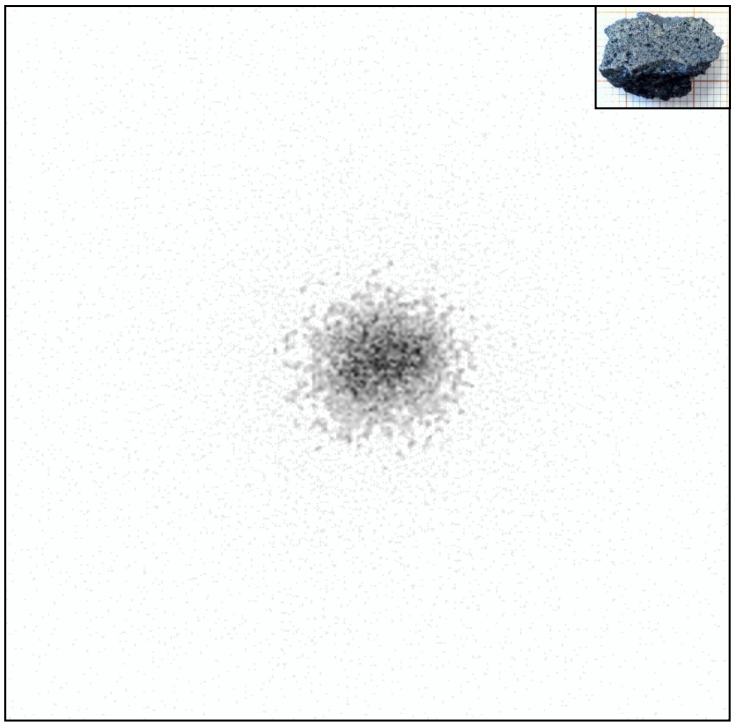

File: d3_7e

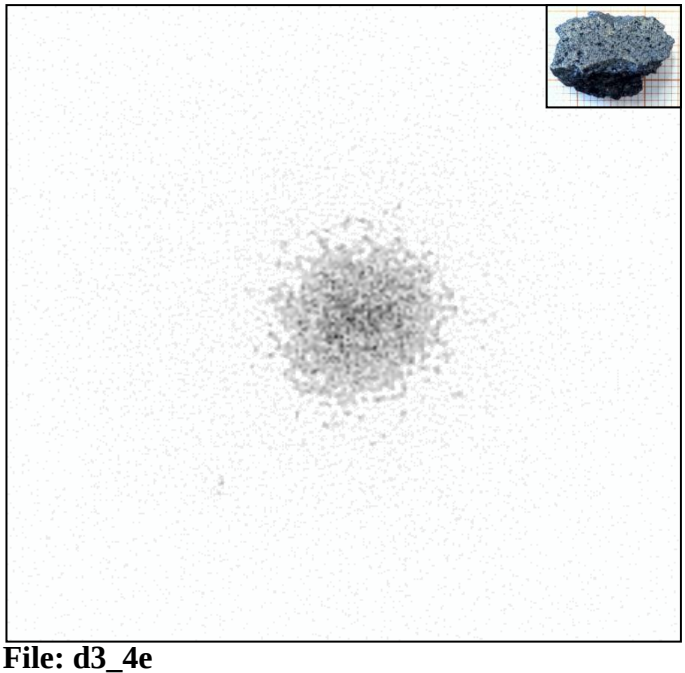

File: d3_4e

5.2.2.2 Uneven side up

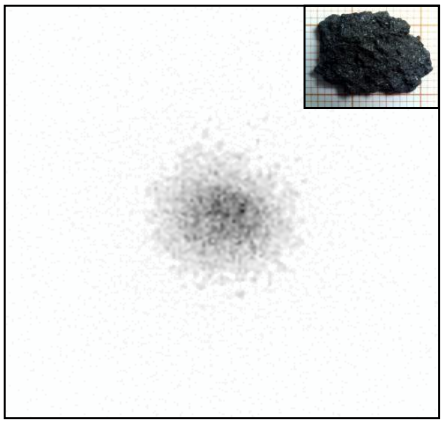

File: d3_wun

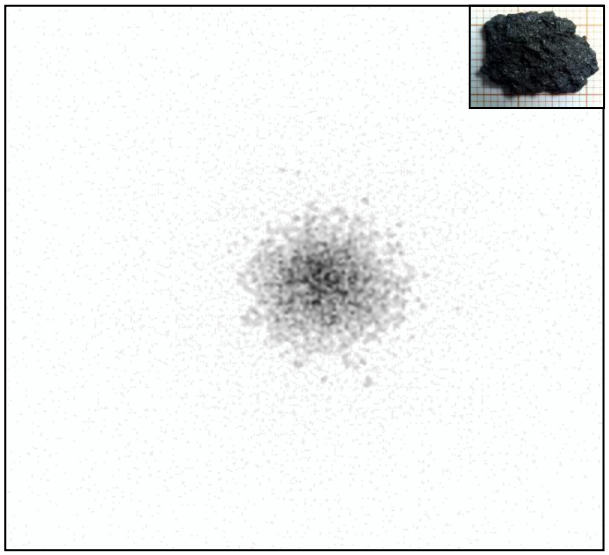

File: d3_1un

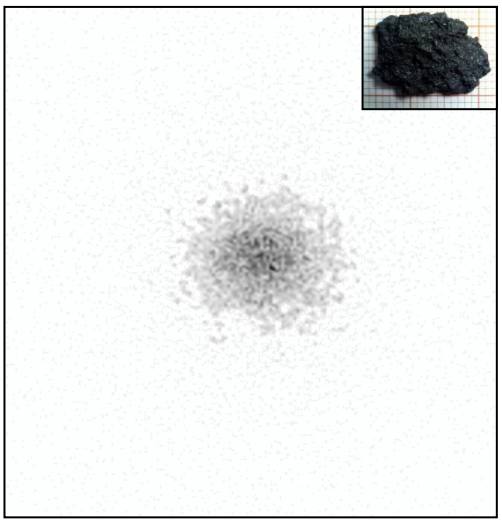

File: d3_2un

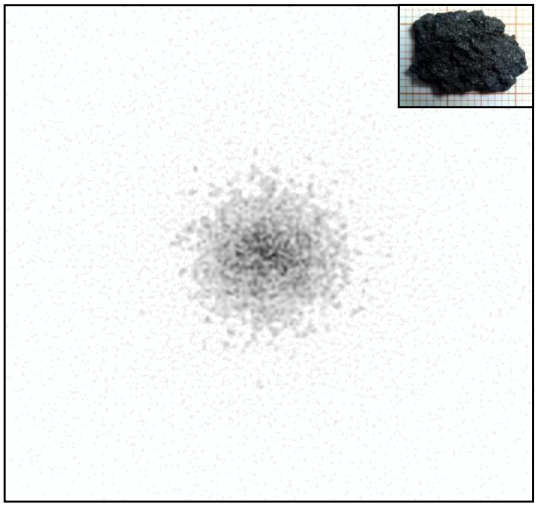

File: d3_3un

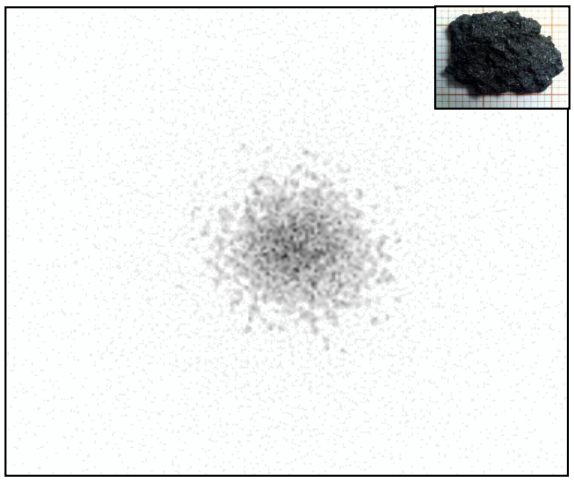

File: d3_5un

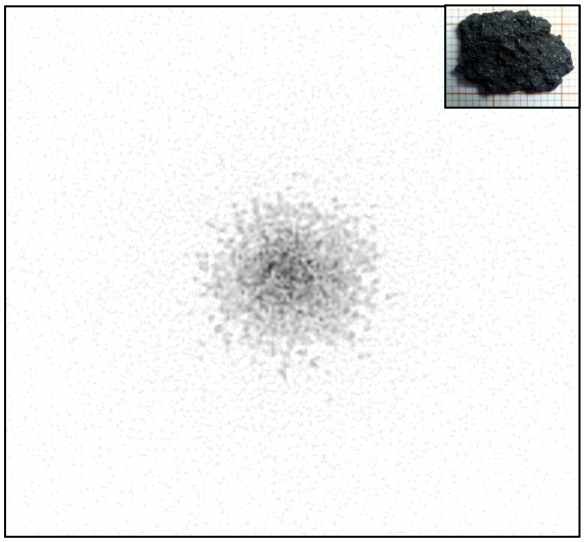

File: d3_7un

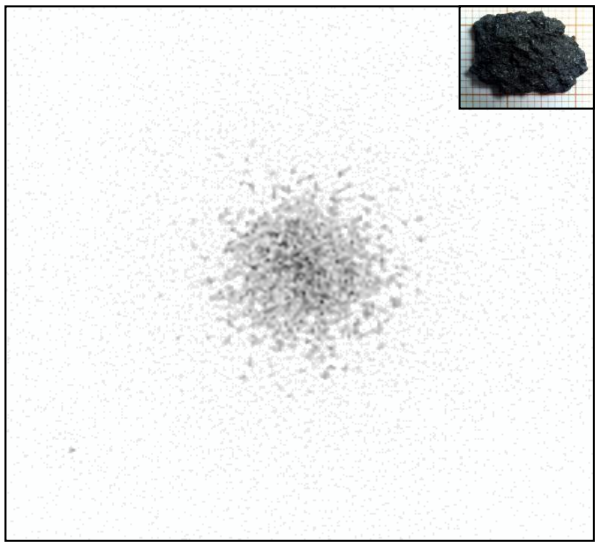

File: d3_4un

5.2.2.3 Subtraction – Even side up [not translated + inverted images]

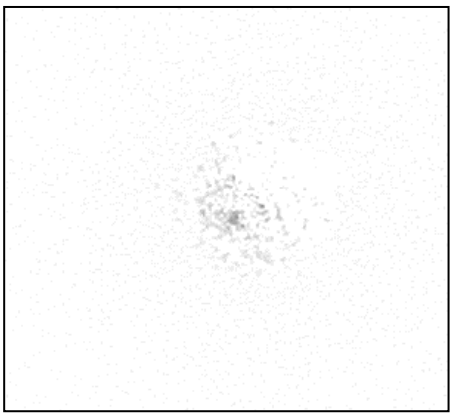

File:Diff_D_e_wm1_ri_nT

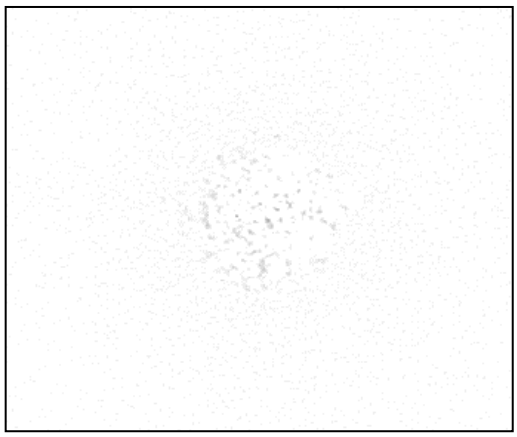

File:Diff_D_e_wm2_ri_nT

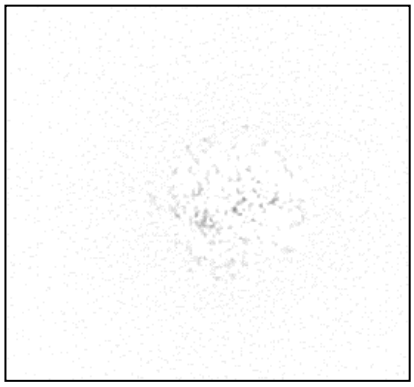

File:Diff_D_e_wm1_ri_nT

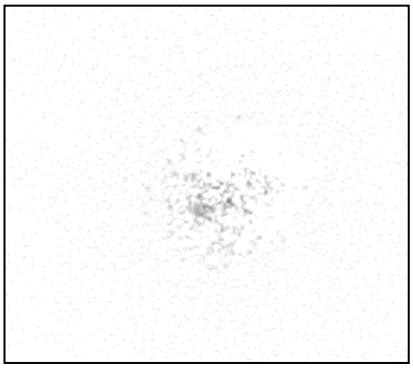

File:Diff_D_e_wm5_ri_nT

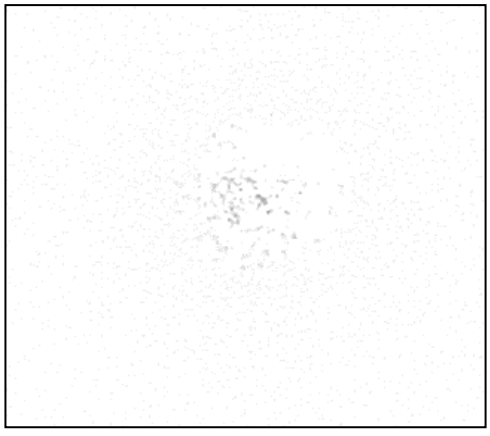

File:Diff_D_e_wm7_ri_nT

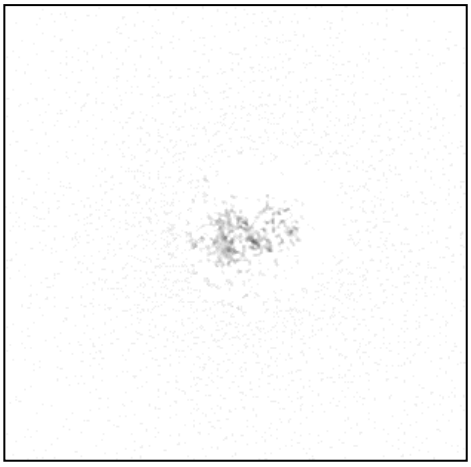

File:Diff_D_e_wm4_ri_nT

5.2.2.4 Subtraction - Even side up [translated + inverted images]

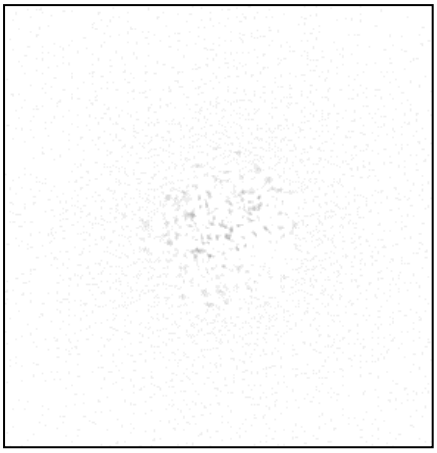

File:Diff_D_e_wm1_ri_T

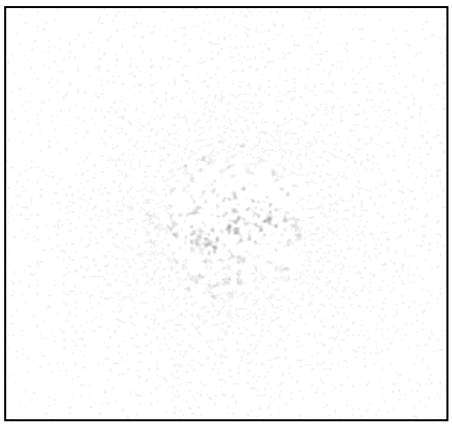

File:Diff_D_e_wm3_ri_T

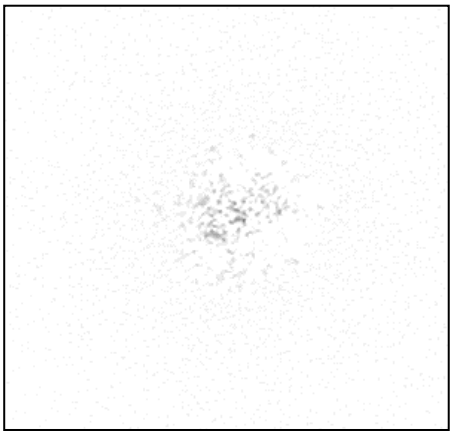

File:Diff_D_e_wm5_ri_T

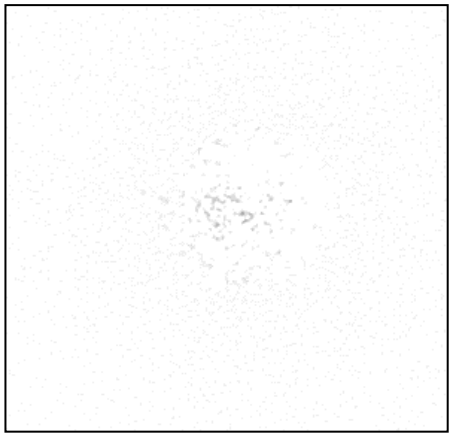

File:Diff_D_e_wm7_ri_T

5.2.2.5 Subtraction - Uneven side up [not translated + inverted images]

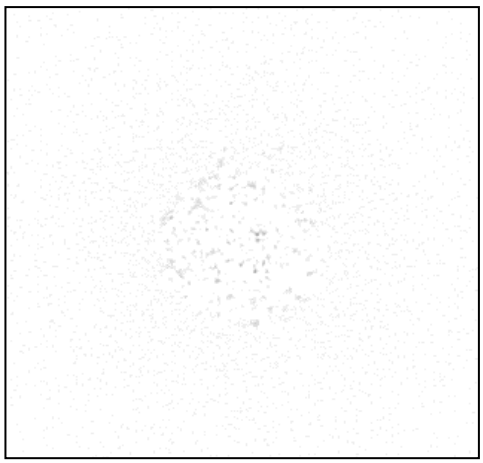

File:Diff_D_un_wm1_ri_T

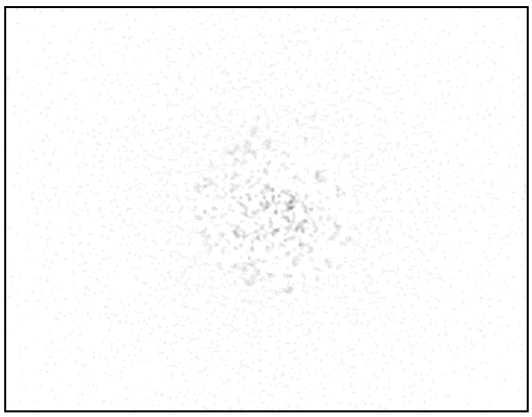

File:Diff_D_un_wm2_ri_T

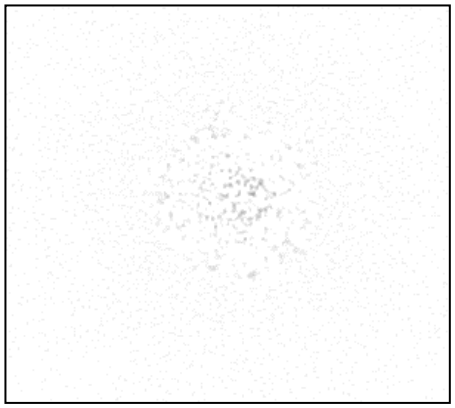

File:Diff_D_un_wm3_ri_T

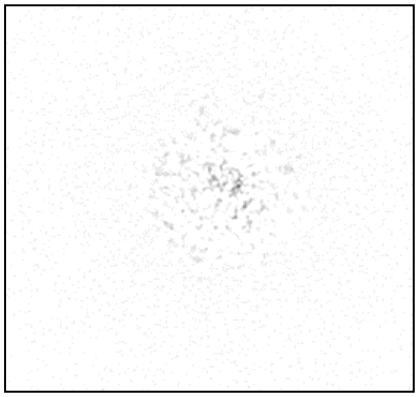

File:Diff_D_un_wm5_ri_T

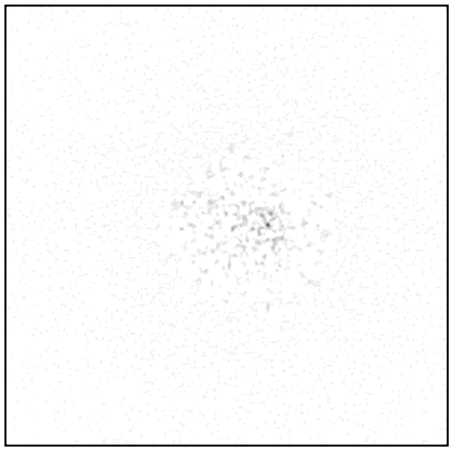

File:Diff_D_un_wm7_ri_T

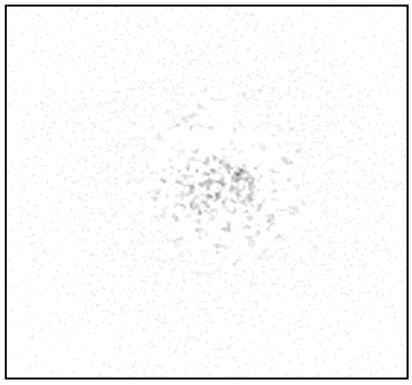

File:Diff_D_un_wm4_ri_T

5.2.2.6 Subtraction - Uneven side up [translated + inverted images]

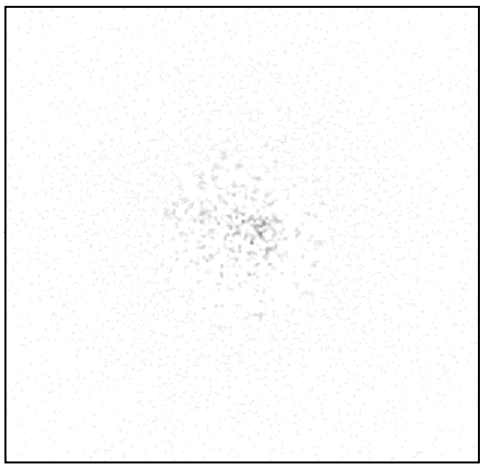

File:Diff_D_un_wm7_ri_T

5.2.3 AVR

5.2.3.1 Even side up

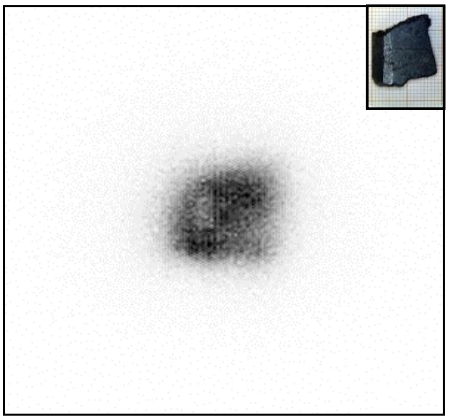

File: 1_a3_we_

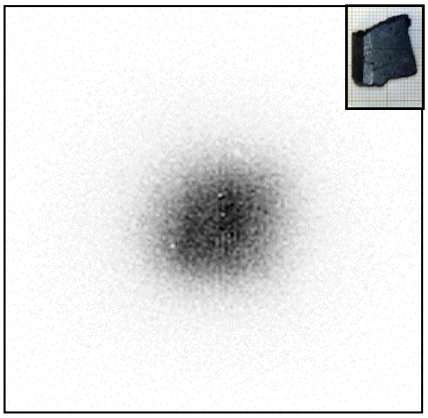

File: 2_a3_1e_

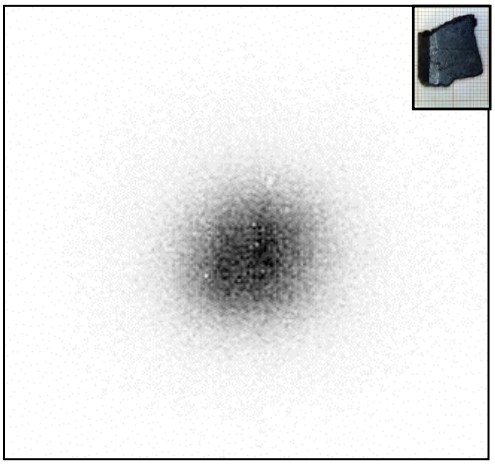

File: 3_a3_2e_

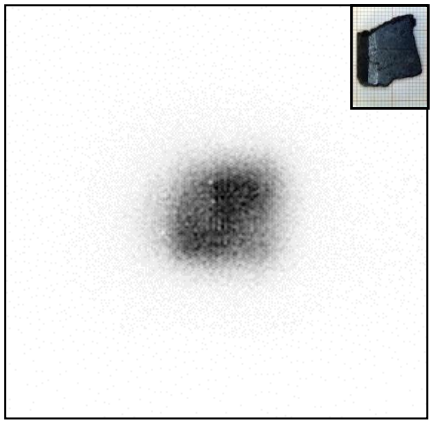

File: 4_a3_3e_

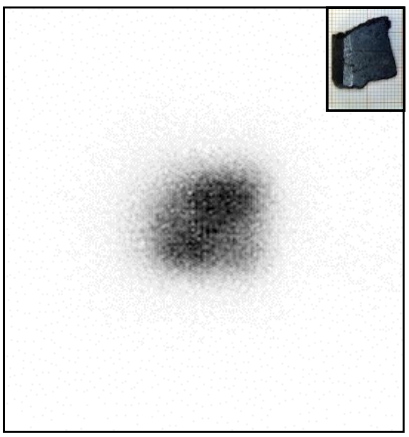

File: 5_a3_5e_

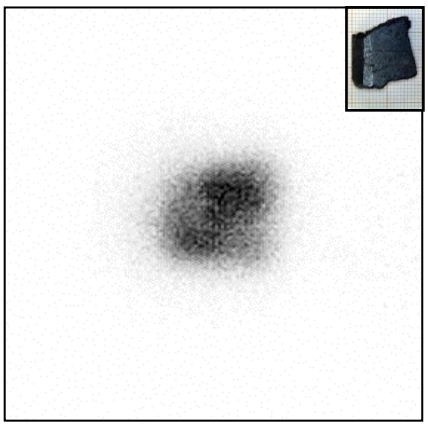

File: 6_a3_7e_

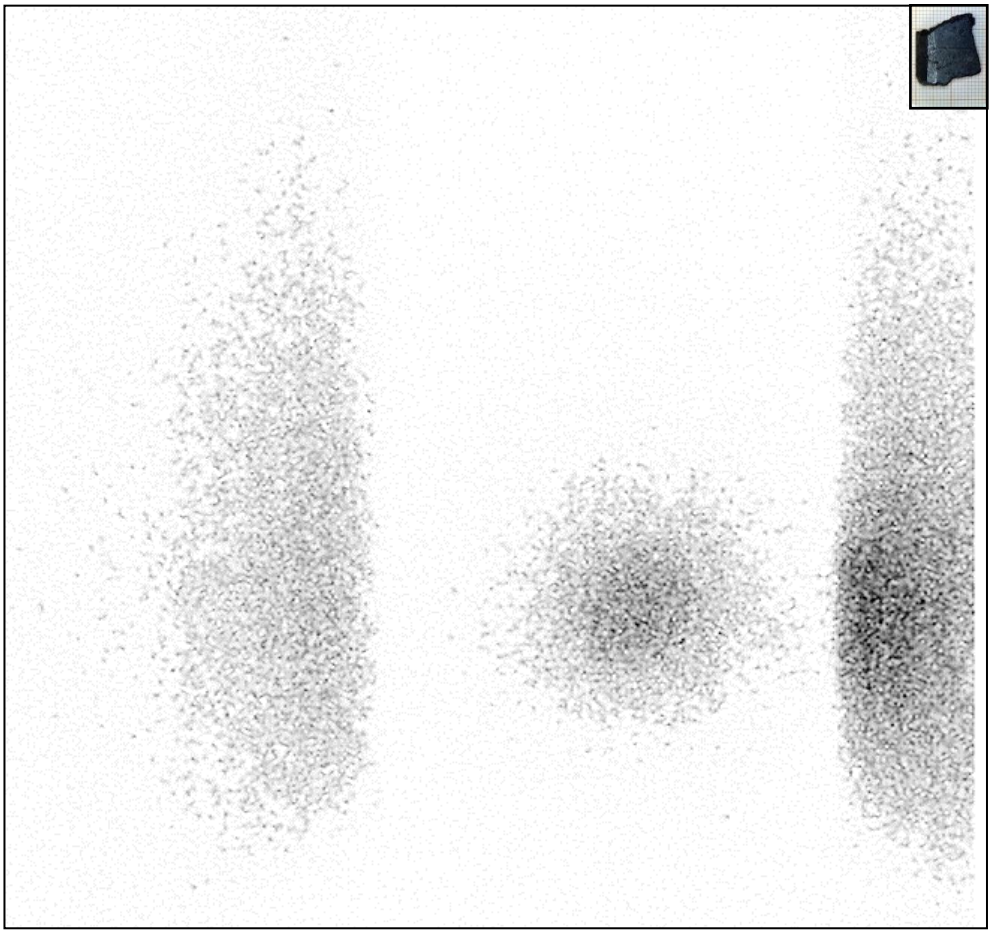

File: 7_a3_4e_

5.2.3.2 Uneven side up

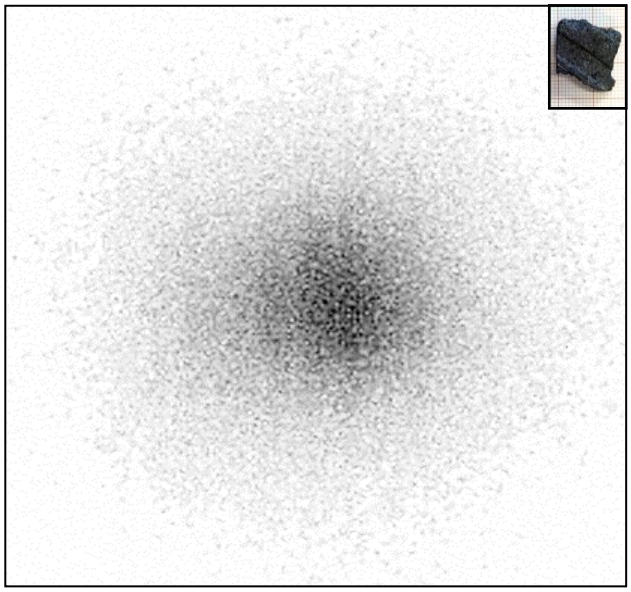

File: 1_a3_wun_

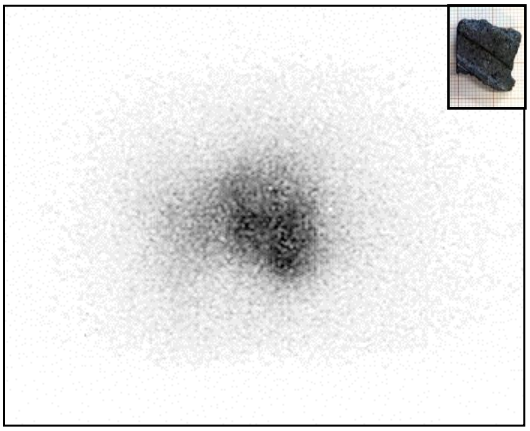

File: 2_a3_1un_

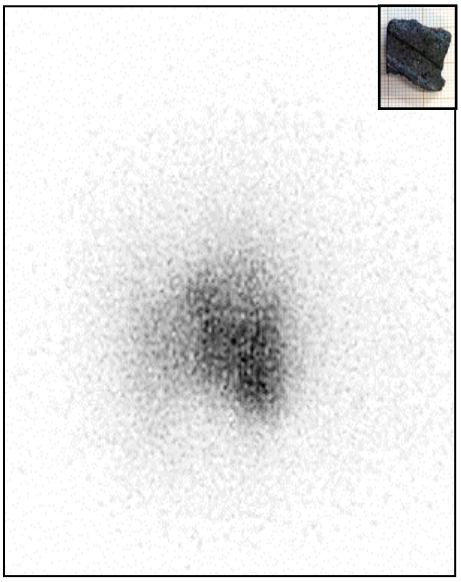

File: 3_a3_2un_

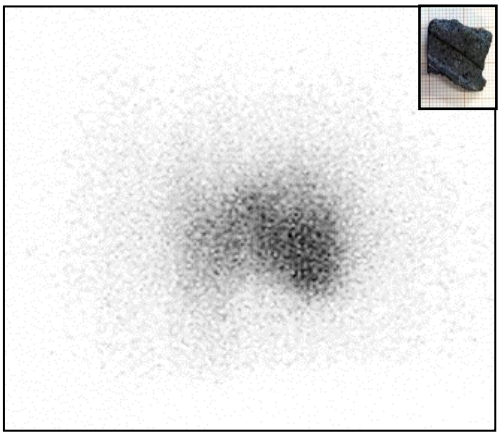

File: 4_a3_3un_

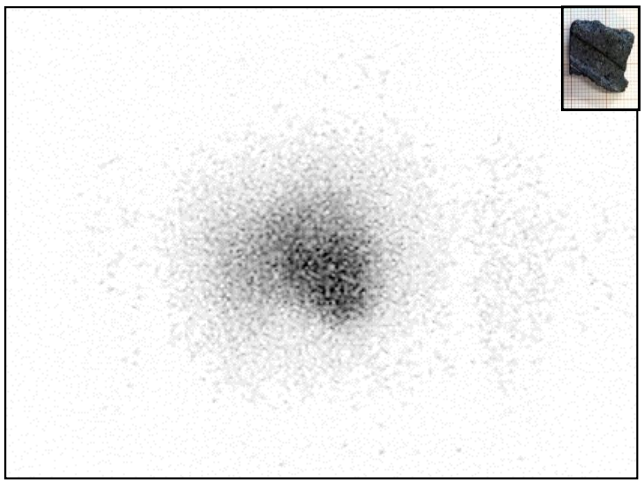

File: 5_a3_5un_

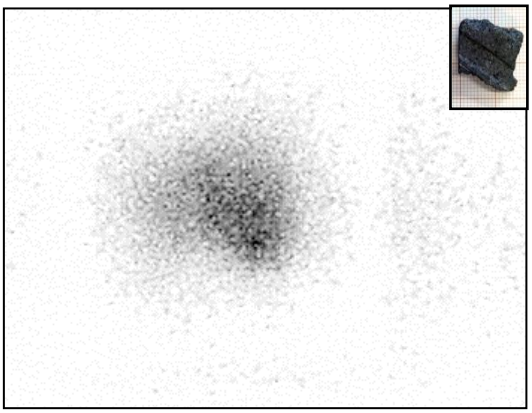

File: 6_a3_7un_

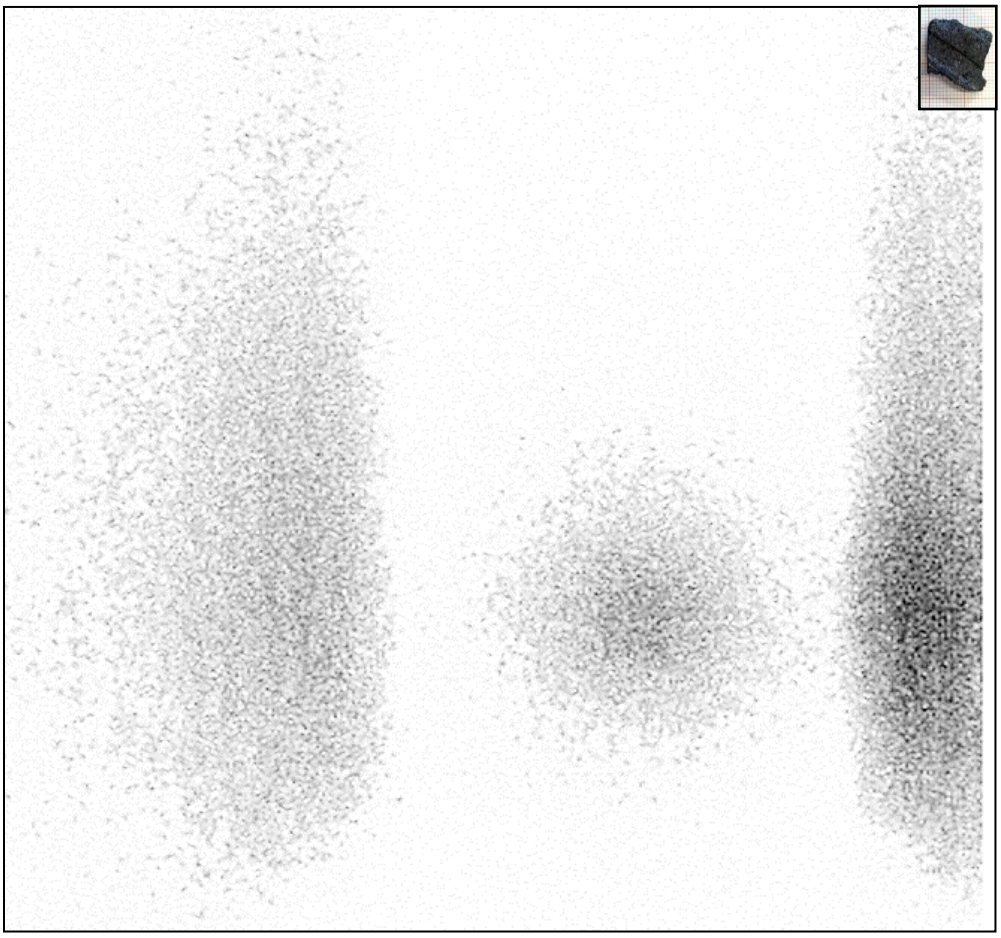

File: 7_a3_4un_

5.2.3.3 Subtraction – Even side up [not translated + inverted]

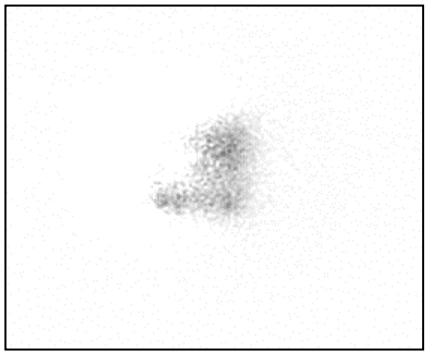

File: Diff_A_e_wm1_ri_nT

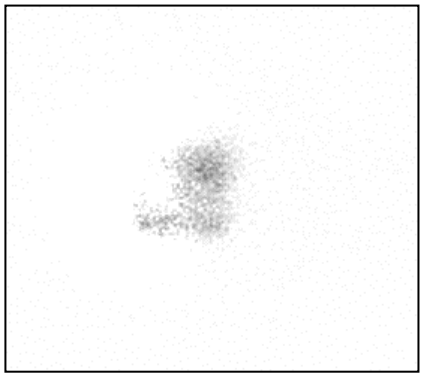

File: Diff_A_e_wm2_ri_nT

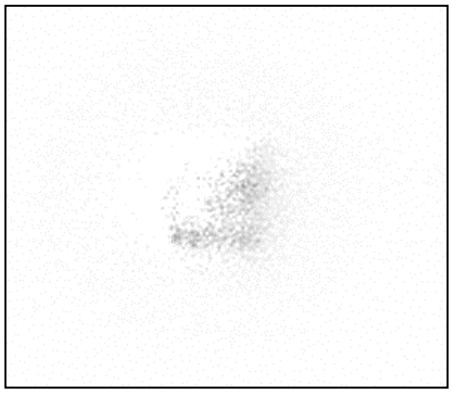

File: Diff_A_e_wm3_ri_nT

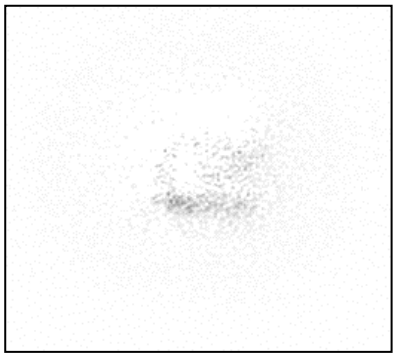

File: Diff_A_e_wm5_ri_nT

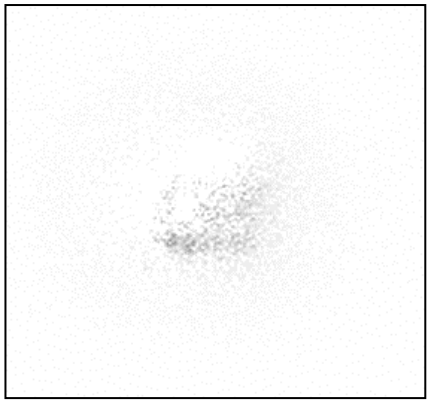

File: Diff_A_e_wm7_ri_nT

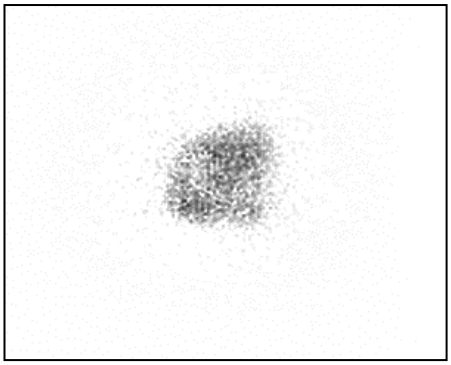

File: Diff_A_e_wm4_ri_nT

5.2.3.4 Subtraction – Even side up [translated + inverted]

No pictures

5.2.3.5 Subtraction – Uneven side up [not translated + inverted]

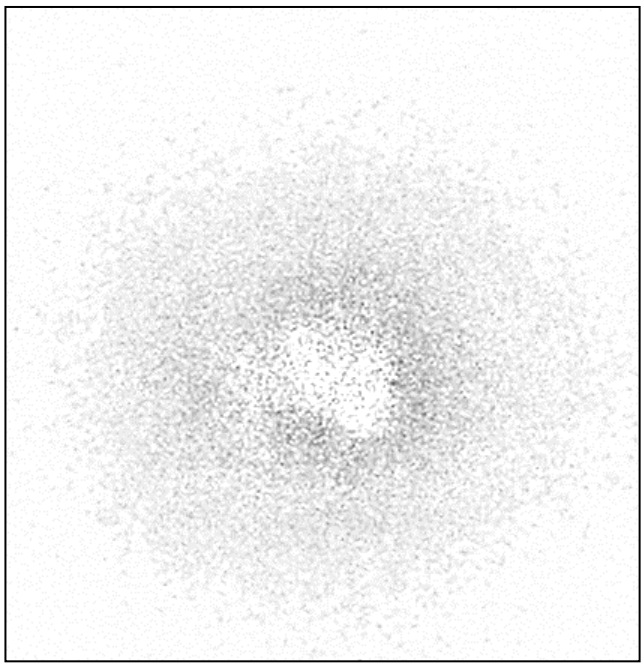

File: Diff_A_un_wm1_ri_nT

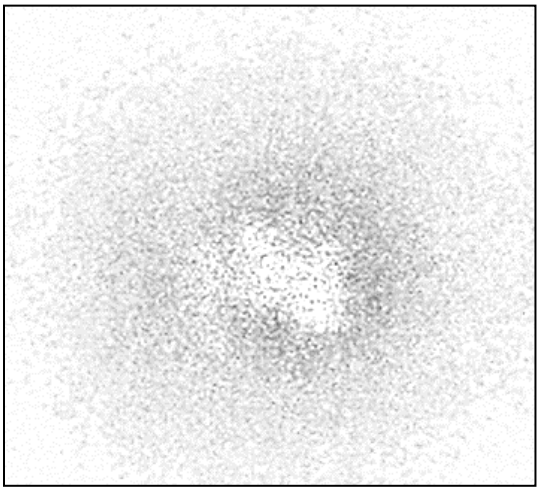

File: Diff_A_un_wm2_ri_nT

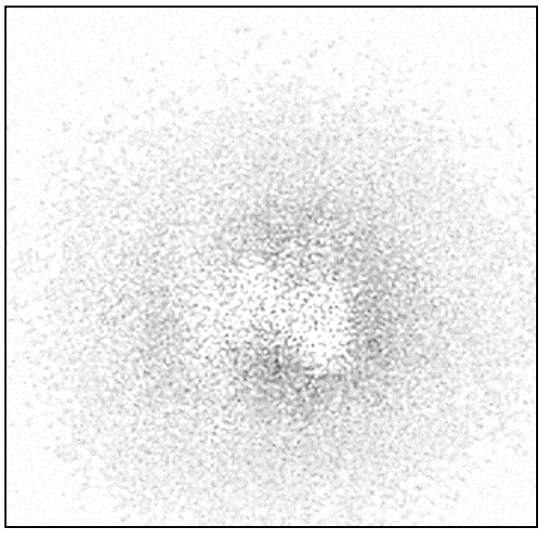

File: Diff_A_un_wm3_ri_nT

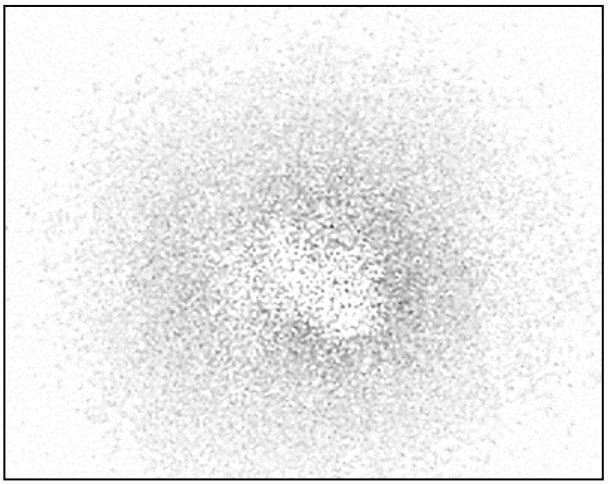

File: Diff_A_un_wm5_ri_nT

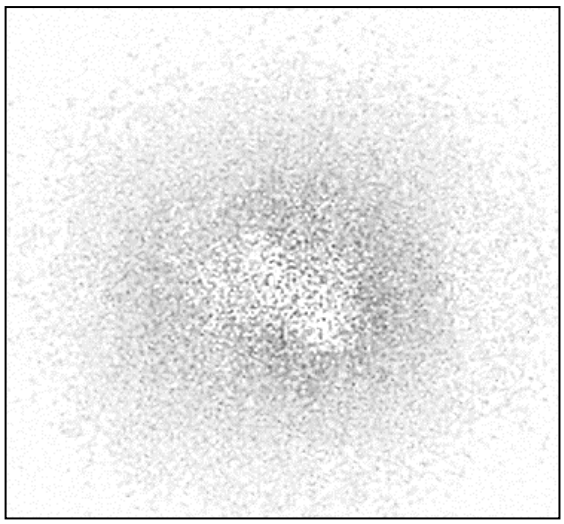

File: Diff_A_un_wm7_ri_nT

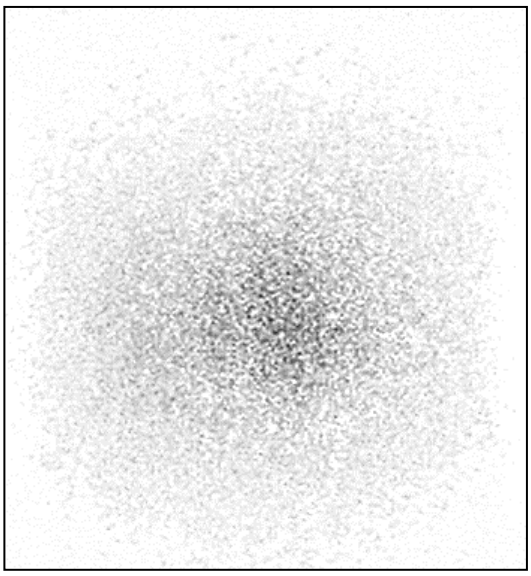

File: Diff_A_un_wm4_ri_nT

5.2.3.6 Subtraction – Uneven side up [translated + inverted]

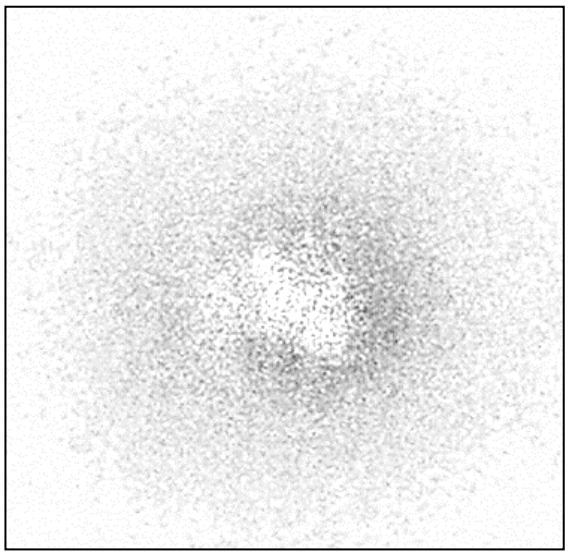

File: Diff_A_un_wm2_ri_T

5.2.4 RBMK

5.2.4.1 Slope side up

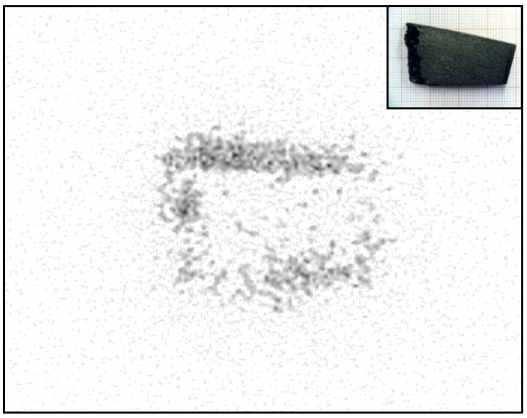

File: r3_3_ws

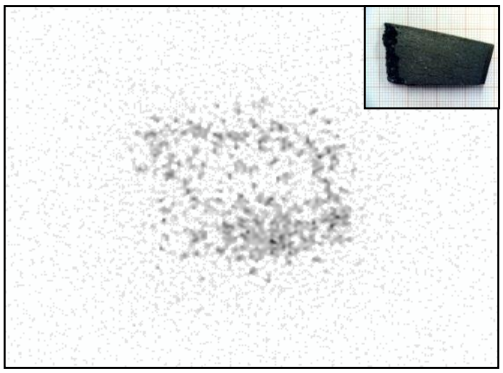

File: r3_3_1s

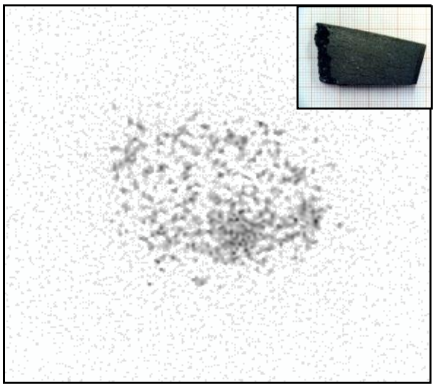

File: r3_3_2s

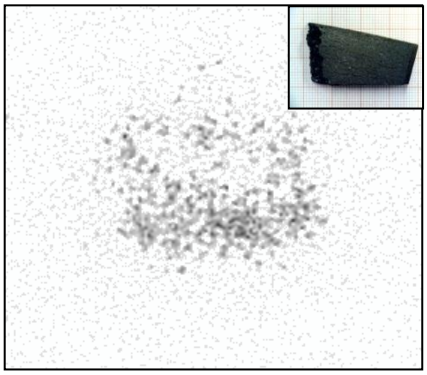

File: r3_3_3s

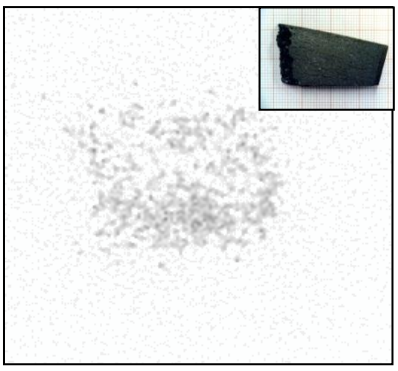

File: r3_3_5s

File: r3_3_7s

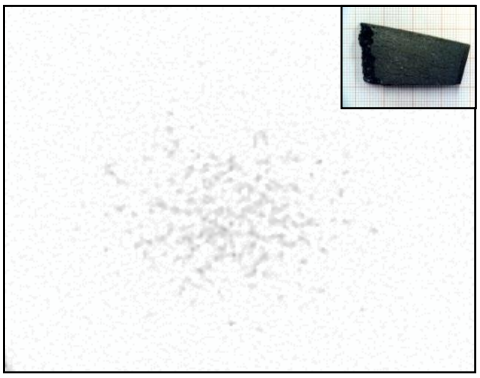

File: r3_3_4s

5.2.4.2 Flat side up

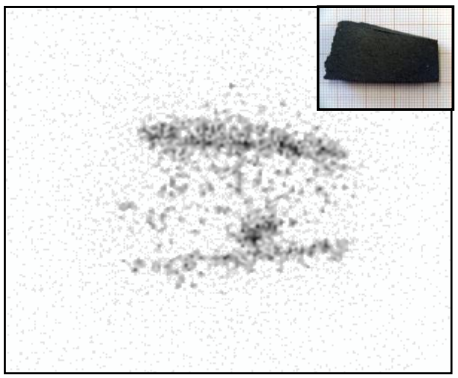

File: r3_3_wf

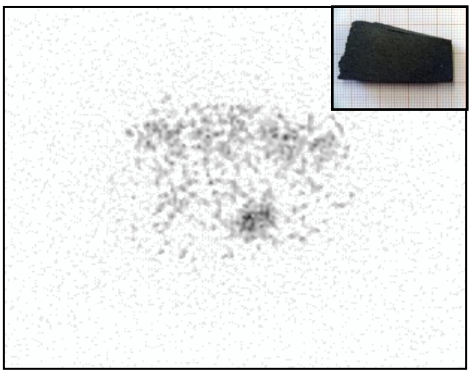

File: r3_3_1f

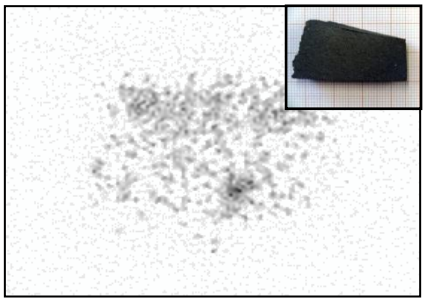

File: r3_3_2f

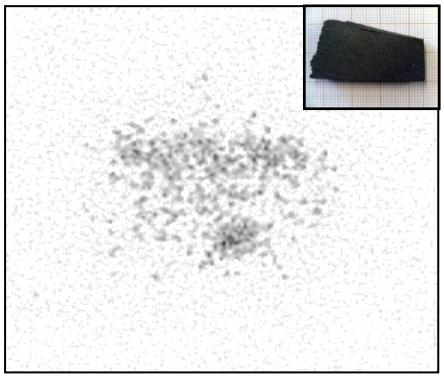

File: r3_3_3f

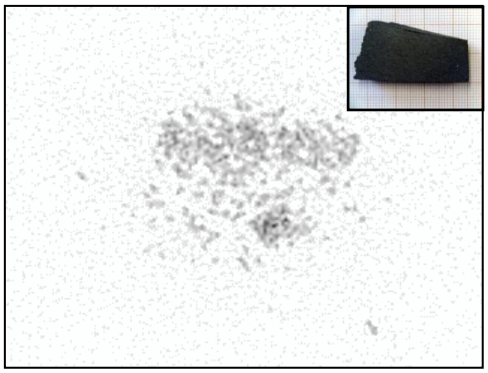

File: r3_3_5f

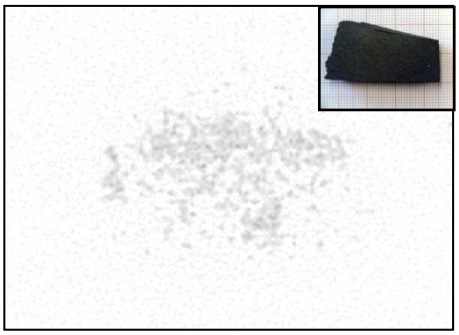

File: r3_3_7f

File: r3_3_4f

5.2.4.3 Subtraction – Slope side up [not translated + inverted]

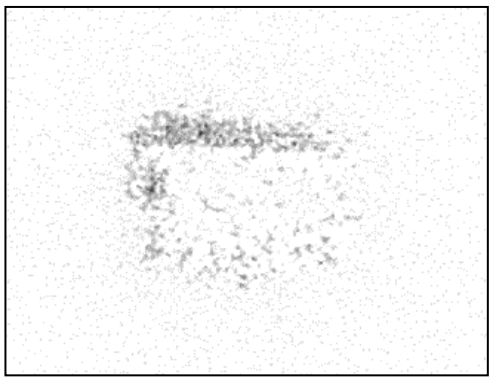

File: Diff_R_s_wm1_ri_nT

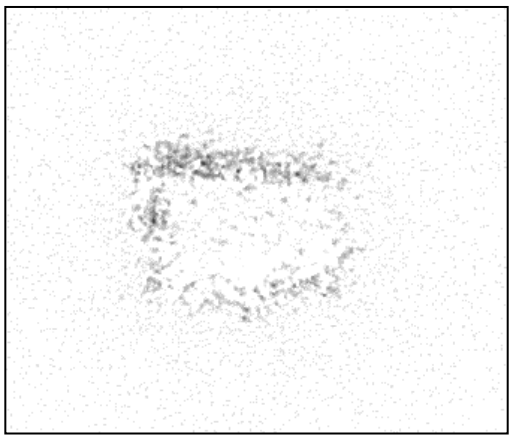

File: Diff_R_s_wm2_ri_nT

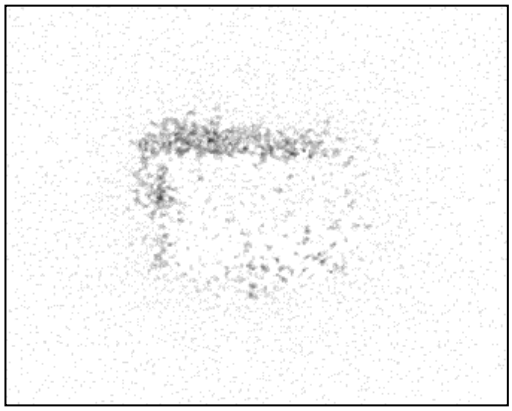

File: Diff_R_s_wm3_ri_nT

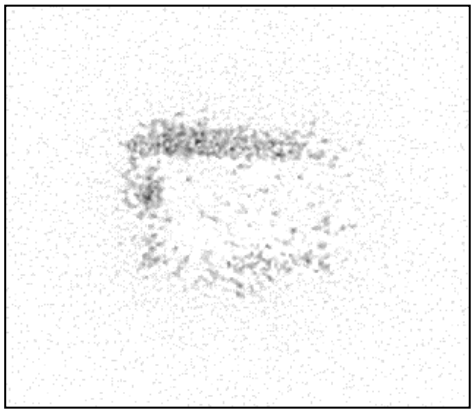

File: Diff_R_s_wm5_ri_nT

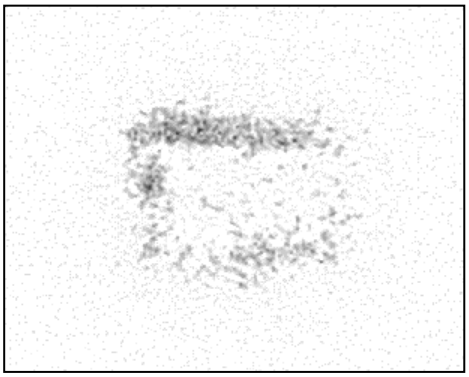

File: Diff_R_s_wm7_ri_nT

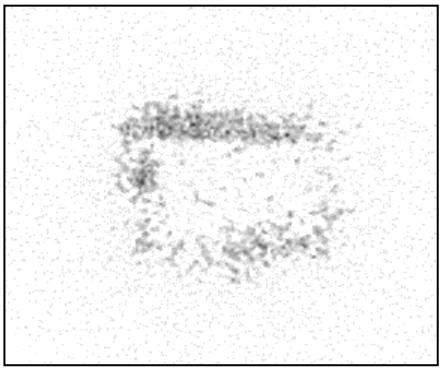

File: Diff_R_s_wm4_ri_nT

5.2.4.4 Subtraction – Slope side up [translated + inverted]

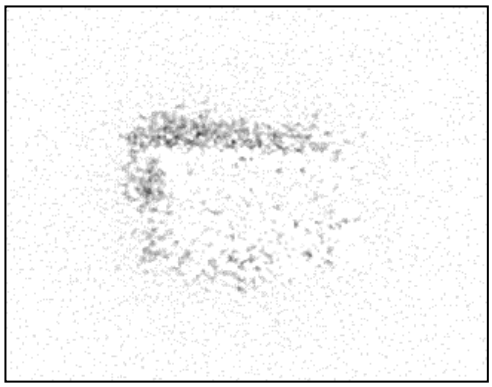

File: Diff_R_s_wm1_ri_T

5.2.4.5 Subtraction – Flat side up [not translated + inverted]

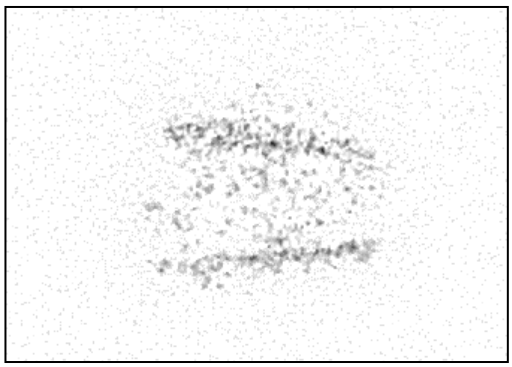

File: Diff_R_f_wm1_ri_nT

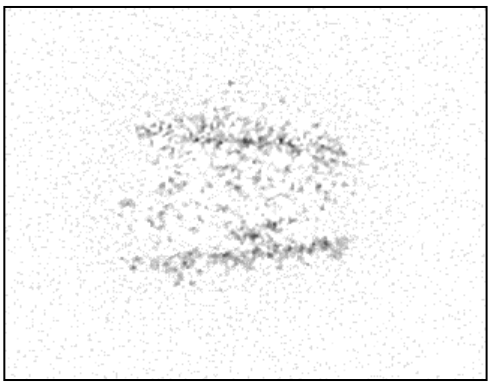

File: Diff_R_f_wm2_ri_nT

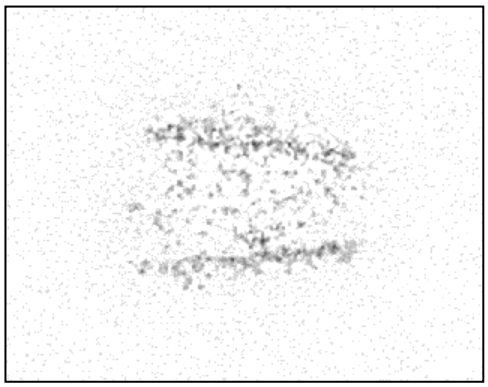

File: Diff_R_f_wm3_ri_nT

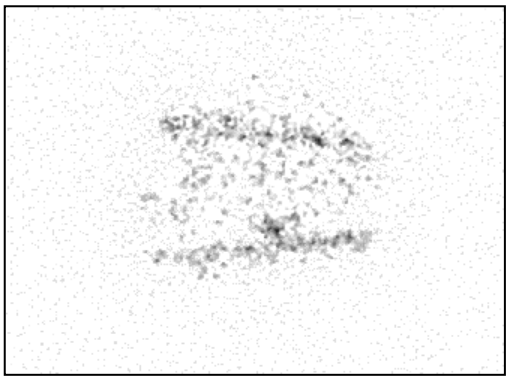

File: Diff_R_f_wm5_ri_nT

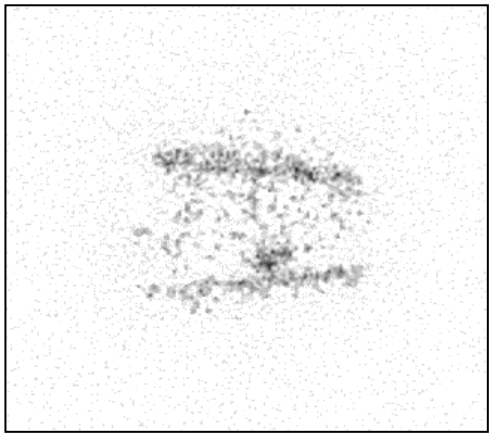

File: Diff_R_f_wm7_ri_nT

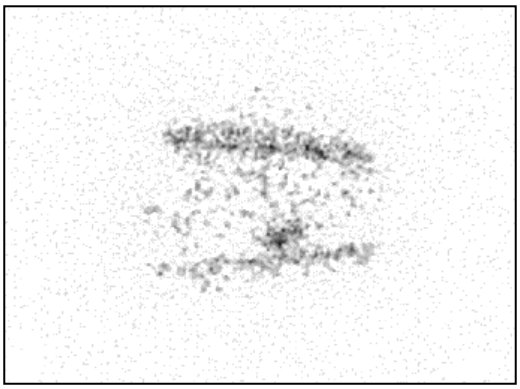

File: Diff_R_f_wm4_ri_nT

5.2.4.6 Subtraction – Flat side up [translated + inverted]

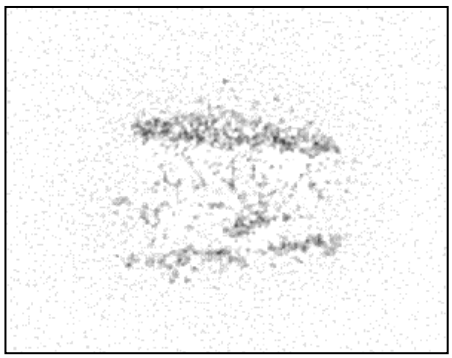

File: Diff_R_f_wm1_ri_nT

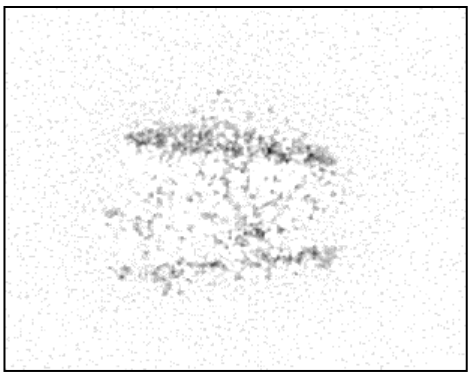

File: Diff_R_f_wm2_ri_nT

5.2.5 MERLIN

5.2.5.1 Vertical line up

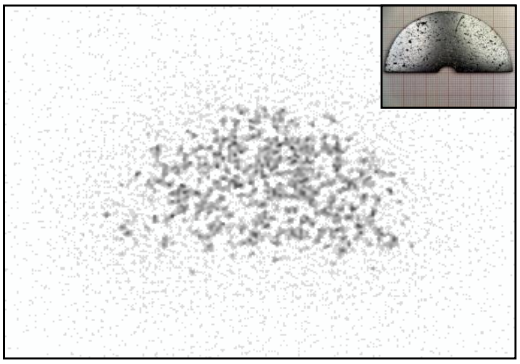

File: m3_wvlu

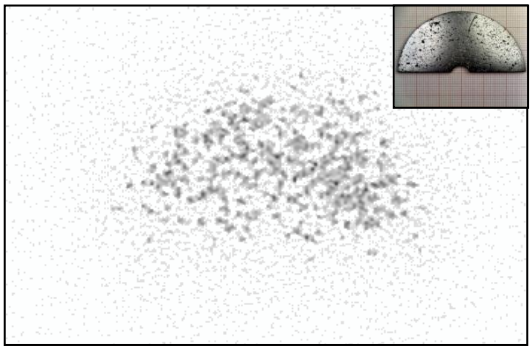

File: m3_1vlu

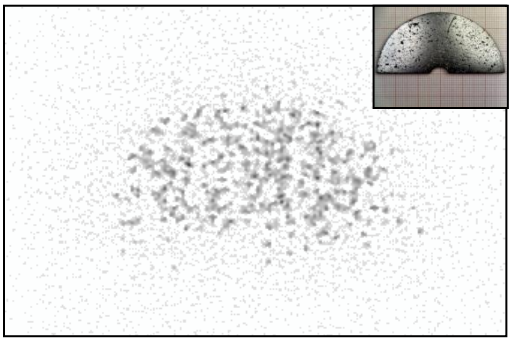

File: m3_2vlu

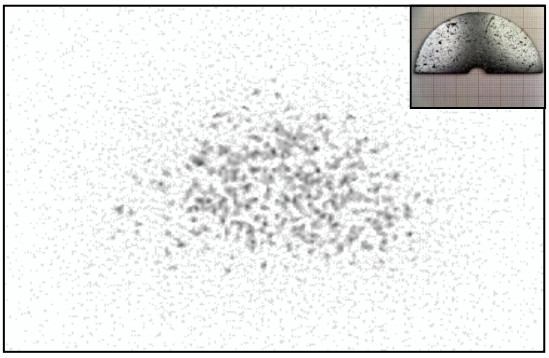

File: m3_3vlu

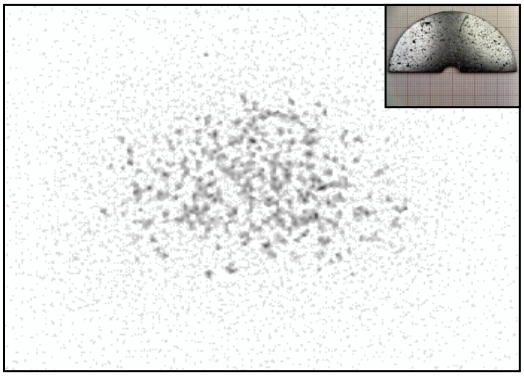

File: m3_5vlu

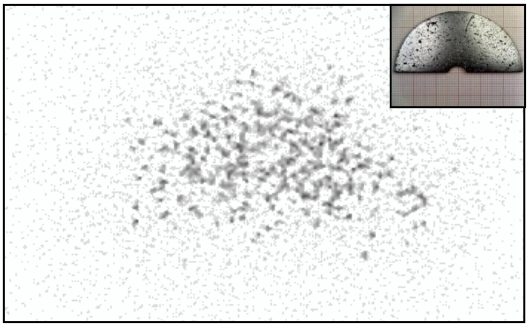

File: m3_7vlu

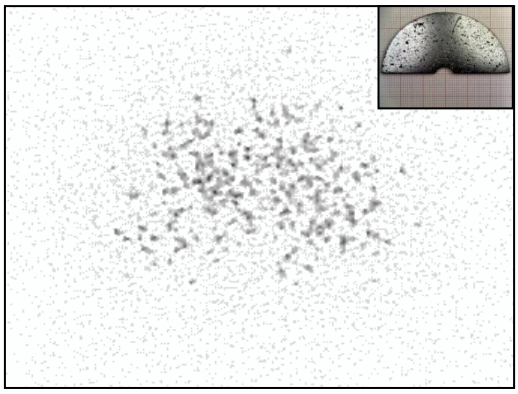

File: m3_4vlu

5.2.5.2 Vertical line down

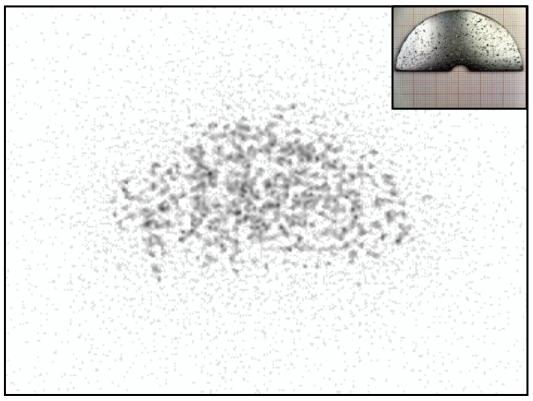

File: m3_wvld

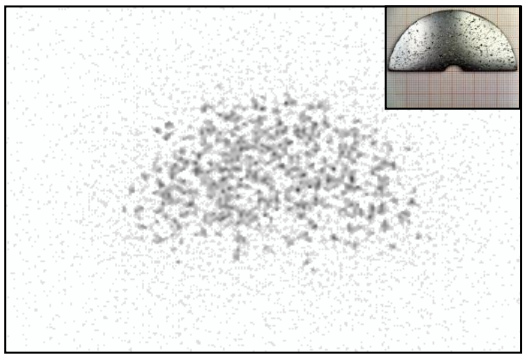

File: m3_1vld

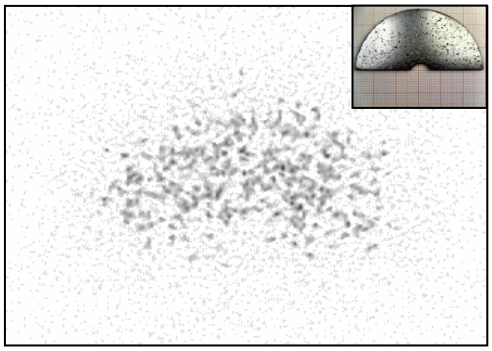

File: m3_2vld

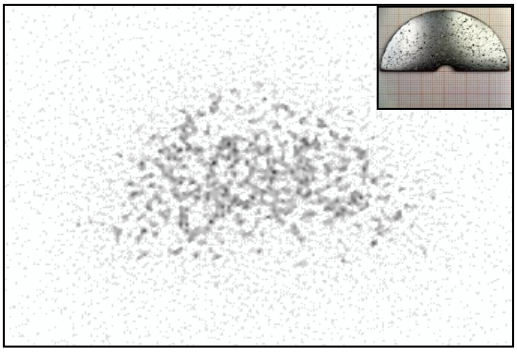

File: m3_3vld

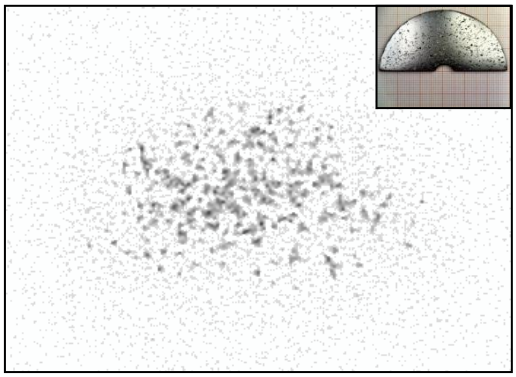

File: m3_5vld

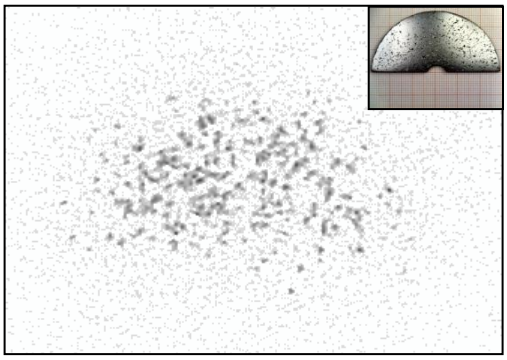

File: m3_7vld

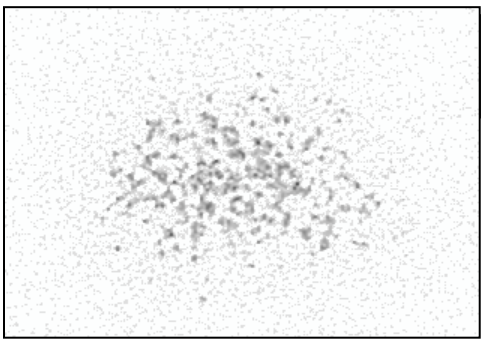

File: m3_4vld

5.2.5.3 Subtraction – vertical line up [not translated + inverted]

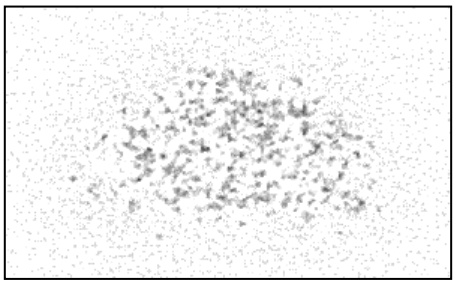

File: Diff_M_vlu_wm1_ri_nT

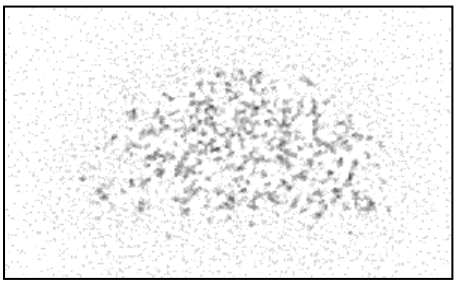

File: Diff_M_vlu_wm2_ri_nT

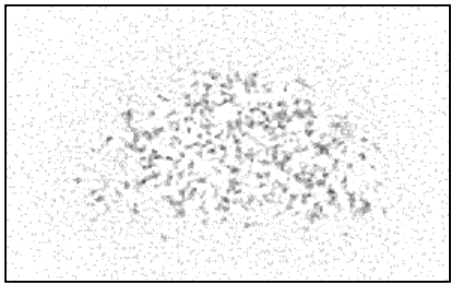

File: Diff_M_vlu_wm3_ri_nT

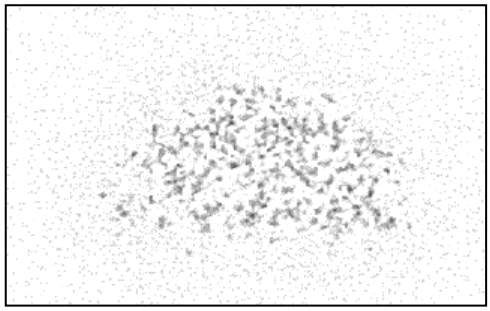

File: Diff_M_vlu_wm5_ri_nT

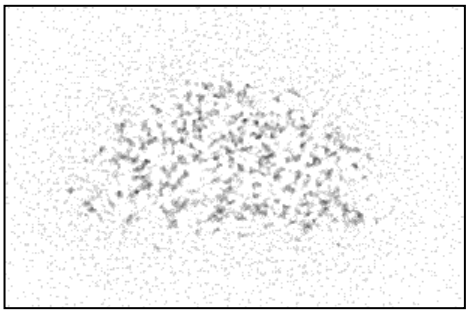

File: Diff_M_vlu_wm7_ri_nT

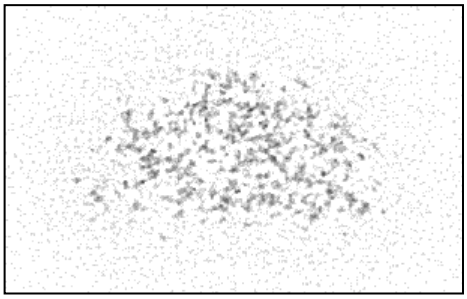

File: Diff_M_vlu_wm7_ri_nT

5.2.5.4 Subtraction – vertical line up [translated + inverted]

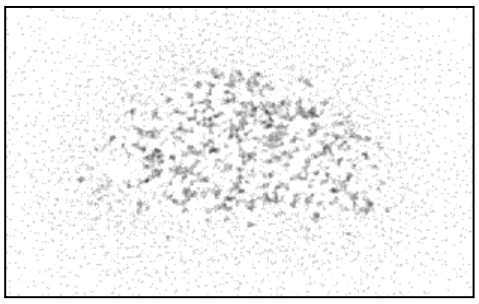

File: Diff_M_vlu_wm1_ri_T

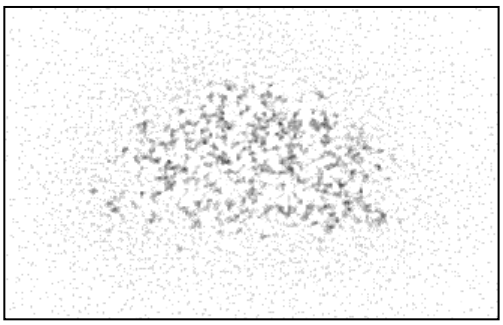

File: Diff_M_vlu_wm5_ri_T

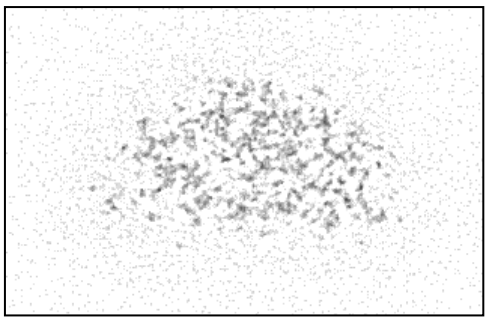

File: Diff_M_vlu_wm4_ri_T

5.2.5.5 Subtraction – vertical line down [not translated + inverted]

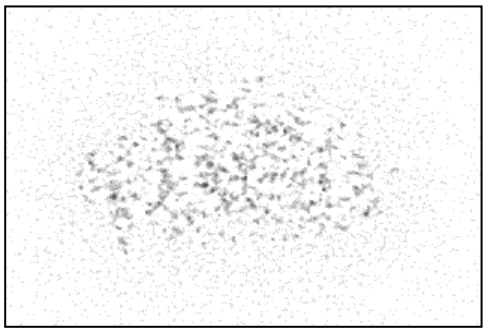

File: Diff_M_vld_wm1_ri_nT

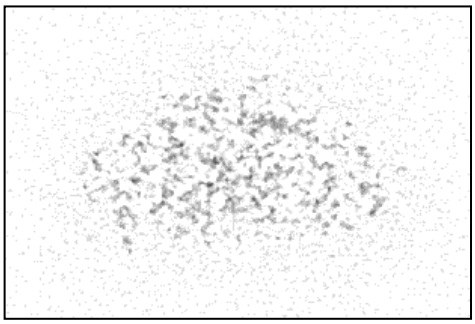

File: Diff_M_vld_wm2_ri_nT

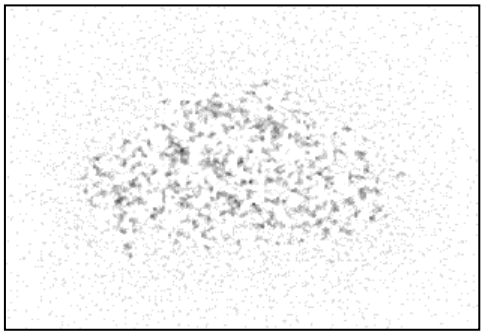

File: Diff_M_vld_wm3_ri_nT

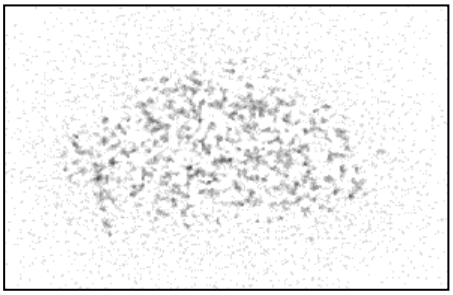

File: Diff_M_vld_wm5_ri_nT

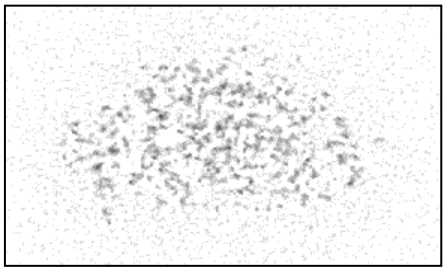

File: Diff_M_vld_wm7_ri_nT

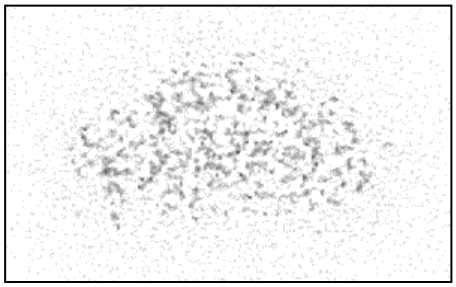

File: Diff_M_vld_wm4_ri_nT

5.2.5.6 Subtraction – vertical line down [translated + inverted]

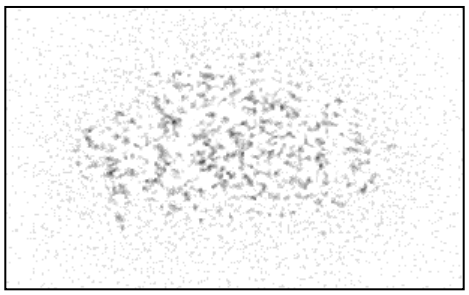

File: Diff_M_vlu_wm1_ri_T

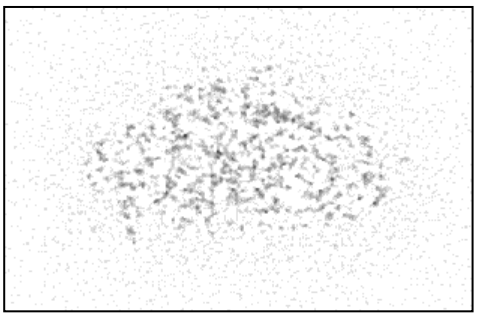

File: Diff_M_vlu_wm2_ri_T

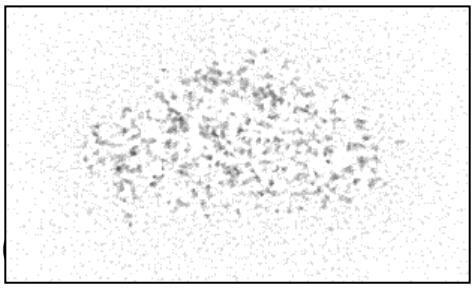

File: Diff_M_vlu_wm3_ri_T

6 Discussion

6.1 SLA

Even Side

The image 1_s3_we_ without an absorber shows active areas in the three corners of the graphite sample.

Image 2_s3_1e_ does not show this areas anymore. As the probe activity mostly consists out of H-3, C-14 and Co-60 (table 3) the absorber (0.1 mm) takes away the radiation of H-3 and C-14.

Images 3_s3_2e_, 4_s3_3e_ and 5_s3_5e_ show no change in the detected activity. An artifact exists at the upper part in all three images. It has nothing to do with the activity distribution of the sample. The detector (Instant-Imager) became, so to speak, temporarily out of order.

Images 3_s3_2e_, 4_s3_3e_ and 5_s3_5e_ show no change in the detected activity. An artifact exists at the upper part in all three images.

Images 6_s3_7e_ and 7_s3_4e_ show no artefacts and no areas of intensive activity.

The circular shaped area around the physical borders of the sample due to beta minus emission increase with higher absorber densities. For the images 1_s3_we_ the circle is smaller and for the images 7_s3_4e_ the circle is bigger than for the rest of the images.

In general you can say that the activity of the even side is distributed mostly homogenously. There are just in the three corners of the sample an accumulation of higher activity areas.

For a better evaluation between of the images between each other the maximum values of the pixels for each sample are listed in following table.

Table 10: Filename of the image with the corresponding min/max value pair for the even side.

Filename	Min/Max value for the pixel
1_s3_we_	0/47
2_s3_1e_	0/33
3_s3_2e_	0/31
4_s3_3e_	0/30
5_s3_5e_	0/29
6_s3_7e_	0/29
7_s3_4e_	0/27

As a short explanation to table 10. The max value affects the brightness/darkness of the image. The lower the value, the darker the seen area in the image. Hence a lower max value can generate the impression of a more radioactive area of the sample.

Uneven side

The image 1_s3_wun_ without an absorber shows also in all three corners areas of higher activities. In comparison to the image of the even side without absorbers the areas are not so big. You can derivate out of this that the activity goes sometimes through the graphite sample.

Image 2_s3_1un_ shows the same effect like for the even side of the sample. Hence the radionuclides whose radiation is absorbed by the absorbers are again H-3 and C-14. Beside the image 2_s3_1un_ also 3_s3_2un_ and 4_s3_3un_ show no significant absorption effect.

Image 5_s3_5un_ in comparison to the other three mentioned images show a little change. Whereas image 5_s3_5un_ and image 6_s3_7un have not experienced an absorption effect too.

Image 7_s3_4un_ with the thickest absorber shows a very homogenous activity distribution. However, it is not understandable why the graphite sample appears in this image more radioactive than for the foregoing images. 5_s3_5r_ and 6_s3_7r_ with the lower area density.

The complete image series shows no artefacts in the sample. Additionally the activity and the radionuclides respectively are distributed homogenously in the sample.

Table 11: Filename of the image with the corresponding min/max value pair for the uneven side.

Filename	Min/Max value for the pixel
1_s3_wun_	0/116
2_s3_1un_	0/30
3_s3_2un_	0/33
4_s3_3un_	0/29
5_s3_5un_	0/39
6_s3_7un_	0/32
7_s3_4un_	0/38

Comparison even/uneven side

Due to the fact that, regarding table 10 and table 11**,** the max values for the pixels are different a satisfying comparison statement is not made here. Darker areas could be interpretated as more radioactive, whereas just a lower maximum value is the reason.

Subtraction of images

The evaluation of the subtraction images is difficult. Despite the fact that with the software ImageJ images were translated to bring them in the same position for the subtraction of each other, there is no 100 per cent assurance that the pixels of two images have the same position. That`s why it is possible that by a subtraction of two images wrong information can be produced.

However, before measuring the graphite sample actions were made to bring it into the same position in the Instant-Imager. For example a mask (figure 28) was used to fix the sample. Bringing this mask into the always same position on the table of the Instant-Imager a rectangle out of paper, also seen in figure 28, was used. Anyhow small displacements (< 1mm) were possible. Because of the lifting up movement of the Instant-Imager, but also due to the fact that the position fixing was done with the eye adjustment. If, for instance, the fixing of the location would be realized with laser beams, what is probably from the complexity not arguable, the location of the samples would be exactly the same.

6.2 DIDO

Even side

Image d3_we without absorber shows a homogenous distribution of the radionuclides.

Image d3_1e shows no strong absorption effect, whereas H-3 is responsible for the most activity. Probably the amount of tritium nuclides is relatively low. Eu-155 and C-14 can be also absorbed, as their beta minus radiation energy is relatively low.

Images d3_2e, d3_3e, d3_5e and d3_7e look roughly the same. Accordingly no absorption took place. Just image d3_5e has a lower intensity.

However the following more intensive appearance of the sample surface by using an thicker absorber is not understood.

The use of the last absorber resulting in image d3_4e has an effect on the emission of radioactive radiation.

The conclusion out of this measurement series is the fact that actually just the last absorber has a strong effect on the absorption of the radioactive radiation. The radionuclides are allocated uniformly over the complete sample.

Table 12: Filename of the image with the corresponding min/max value pair for the

Filename	Min/Max value for the pixel
d3_we	0/25
d3_1e	0/19
d3_2e	0/16
d3_3e	0/16
d3_5e	0/16
d3_7e	0/13
d3_4e	0/13

Uneven side

Image d3_wun without an absorber shows a homogenous arranged radionuclide inventory.

The effect of the first absorber can not be derived by the intensity of the radioactive areas. The reason for this are the different max values for pixels of image d3_wun and d3_1un. The max value for the first image is 25. For the second image 13, consequently the pixels appear more radioactive in the second image whereas there is no more radioactivity.

Images d3_2un, d3_3un, d3_5un and d3_7un have no absorption effect. Just the jump from image d3_1un to d3_2un is result of an absorption. Due to the relative huge amount of radionuclides in the sample it is not easy to find out which radionuclides were absorbed. I assume a little bit Co-60 (beta minus energy: 0.3 MeV), Cs-137 (0.5 MeV) and Eu-154 (0.6 MeV).

The last image d3_4un shows a small absorption effect. Perhaps Cs-134 (0.7 MeV), Co-60 (1.5 MeV) and Cs-137 (1.2 MeV) is partly absorbed.

Table 13: Filename of the image with the corresponding min/max value pair for the

Filename	Min/Max value for the pixel
d3_wun	0/25
d3_1un	0/15
d3_2un	0/18
d3_3un	0/16
d3_5un	0/15
d3_7un	0/16
d3_4un	0/12

Comparison even/uneven side

No special regions of higher activity exist on both sides. The radionuclides are allocated uniformly. Also the effect of the several absorbers for both sides is the same. By using the first absorber a part of the emitting radiation is absorbed. From then on (d3_1un/d3_1e) to (d3_7un/d3_7e) the absorbers have no significant impact on the absorption of the radiation.

For me the fact that the shown activity in image d3_7e is higher as in the image d3_5e, with a thicker absorber, is not understandable. The max values of the pixels can not be the reason as they have for both images the same value.

Subtraction of images

See discussion for the SLA sample

6.3 AVR

Even side

In image 1_a3_we without absorber can be seen an area with lower activity then the rest of the sample.

In images 2_a3_1e_ and 3_a3_2e_ no big change in the activity is observed. In comparison to the first image without absorber these is a little absorption effect which is probably the absorbed radiation of tritium and you can be sure that the mentioned area in image 1_a3_we contains H-3 (beta minus energy: 0.02 MeV) and perhaps C-14 (0.2 MeV) and Eu-155 (0.17 MeV). In the lower left area of the graphite sample an artifact exists.

For the following three images 4_a3_3e_, 5_a3_5e_ and 6_a3_7e_ no absorption effect is displayed.

In image 7_a3_4e_ the absorption effect is shown. The rectangular shaped vertical areas on both sides of the sample consist of Y-90 radiation.

As a general conclusion can be said that the radionuclides are arranged homogenously.

Table 14: Filename of the image with the corresponding min/max value pair for the

Filename	Min/Max value of the pixel
1_a3_we_	0/286
2_a3_1e_	0/210
3_a3_2e_	0/164
4_a3_3e_	0/232
5_a3_5e_	0/180
6_a3_7e_	0/150
7_a3_4e_	0/23

Uneven side

Image 1_a3_wun shows no structure but a relative big, circular shaped area of radiation.

After the use of the first absorber the structure of the graphite sample is clearer. I do not understand why the sample appears clearer after the use of the absorbers.

The remaining images 2_a3_1un, 3_a3_2un, 4_a3_3un, 5_a3_5un and 6_a3_7un show no absorption effect.

Just in image 7_a3_4un an absorption, followed with creating two vertical radiation areas around the sample, is displayed.

Thus Sr-90 and Y-90 (beta minus energy: 2.3 MeV) respectively are the main components of the detected radioactivity.

Also in the AVR sample the radionuclides are distributed uniformly.

Table 15: Filename of the image with the corresponding min/max value pair for the

Filename	Min/Max value of the pixel
1_a3_wun_	0/48
2_a3_1un_	0/83
3_a3_2un_	0/75
4_a3_3un_	0/67
5_a3_5un_	0/48
6_a3_7un_	0/43
7_a3_4un_	0/28

Comparison even/uneven side

Comparing both sides you can say that the even side contains probably more radionuclides than the uneven side. Additionally you can mention that the area on the left side of the sample in image 1_a3_we can not be seen in image 1_a3_wun_. Therefore this structure does not go completely through the graphite sample.

Subtraction of images

See discussion for the SLA sample

6.4 RBMK

Slope side

The image r3_3_ws shows a hot spot on the left side of the sample near the slope. The upper edge of the graphite sample emits more radioactive radiation than the lower edge. The surface of the graphite sample has a comparable low radioactivity. This is an evidence for the fact that the radionuclides, mostly C-14, are present on the side areas of the graphite sample.

Image r3_3_is has a far weaker hot spot on the left side. Hence the radioactive area consists mostly of C-14 which is absorbed by the first absorber. The emission of radiation at the upper edge has also almost disappeared. A proof for the existence of low energy beta minus radiation being absorbed by the first absorber. It is unclear why the surface now shows more radioactive spots than at the image without using any absorber.

Images r3_3_2s and r3_3_3s just differ in the dimensions of the non-active area. This area is for the absorber used in r3_3_3s larger than in image r3_3_2s. Both images have in common the more radioactive region at the lower horizontal edge. Interesting is the fact that in image r3_3_ws this part of the sample shows less radioactivity.

Image r3_3_5s has the same radionuclide distribution as it is in image r3_3_3s. Just the brightness of the radioactive areas in the images differs. This is due to different max values for the displayed pixels. Also the distribution of the radionuclides in image r3_3_7s is similar to the one in r3_3_3s and r3_3_3s.

Image r3_3_4s shows no physical borders of the graphite sample.

In general you can say that the radionuclides, mostly C-14, is distributed inhomogeneously.

The dots in the images r3_3_1s through r3_3_4s represent no active areas of the sample.

Table 16: Filename of the image with the corresponding min/max value pair for the

Filename	Min/Max value for the pixel
r3_3_ws	0/10
r3_3_1s	0/9
r3_3_2s	0/8
r3_3_3s	0/8
r3_3_5s	0/15
r3_3_7s	0/24
r3_3_4s	0/21

Flat side

Image r3_3_wf shows an intensive emission of radioactive radiation out of the upper edge. Near the lower edge there is a region with higher radioactive emission. The rest of the surface of the graphite sample has an inhomogeneous allocation of radioactivity.

Due to the fact that in image r3_3_1f the lower edge of the sample disappeared and that the upper edge became weaker in its intensity the low beta minus radiation was absorbed. Hence the effect of C-14 disappeared.

If you look at image r3_3_2f just the circular region of emission over the lower edge of the sample became weaker in its intensity. There are no other differences between the two images.

The same effect can be observed in the images r3_3_3f and r3_3_5f. Just the intensity of the circular radioactive area above the lower edge became a little weaker. On the rest of the surface no great change developed.

In image r3_3_7f and r3_3_4f the effect of the absorbers is obvious. Regarding the radionuclide inventory of the graphite sample (table 5) Co-60 should be absorbed. As the circular shaped radio-active area is not present anymore in the two images. Therefore this area consists of, in my opinion, out of C-60.

Table 17: Filename of the image with the corresponding min/max value pair for the flat

Filename	Min/Max value for the pixel
r3_3_wf	0/20
r3_3_1f	0/11
r3_3_2f	0/11
r3_3_3f	0/10
r3_3_5f	0/11
r3_3_7f	0/21
r3_3_4f	0/9

In general you can say that the activity is distributed inhomogeneously.

Also in this measurement series radioactive dots near the sample not on the sample, appear. Those have nothing to do with the radioactive property of the sample. The conversion of the image to the TIFF type was the reason.

Comparing slope/flat side

On both sides the radionuclides, not being present in a great amount, are distributed inhomogeneously.

Both sides own a region of higher radioactivity. For the slope side this region is located on the slope side. For the flat side this region exists above the lower horizontal edge of the sample.

For the slope side this region consists of C-14. In the case of the flat side C-14 is also present but not the only radionuclide. It is supposed that Co-60 is another component at this area.

Subtraction of images

See discussion for the SLA sample

6.5 MERLIN

Side with vertical line up

Image m3_wvlu has the same radionuclide distribution as it is for the other side oft he graphite sample.

The effect of the first absorber displayed in image m3_1vlu is the same as it is for the other side of the sample. The radiation of H-3 is probably filtered out.

In the remaining images m3_2vlu, m3_3vlu, m3_5vlu and m3_7vlu the absorption effect does not exist. Hence this side of the sample contains a huge amount of radionuclides with higher beta minus energy and gamma radiation.

Just the last absorber in image m3_4vlu absorbs again a little radiation of some radionuclides.

You can conclude that the radionuclides are distributed in the same way like for the other side.

Table 18: Filename of the image with the corresponding min/max value pair for the side with the vertical line up.

Filename	Min/Max value of the pixel
m3_wvlu	0/7
m3_1vlu	0/8
m3_2vlu	0/8
m3_3vlu	0/8
m3_5vlu	0/8
m3_7vlu	0/7
m3_4vlu	0/7

Side with vertical line down

Image m3_wvlu shows a relatively uniform distribution of the radionuclides in the sample.

The absorber in image m3_1wvld took away a little bit of the radionuclide H-3.

In image m3_2wvld additional radiation is absorbed, probably C-14.

The radionuclide distribution in image m3_3wvld seems more intensive than in the image with a thinner absorber.

The last three images m3_5wvld, m3_7wvld and m3_4wvld have not significant change in the shown activity of the radionuclides.

In general you can say that the radionuclides are distributed homogenously and that the activity is concentrated in granulate shaped areas.

Table 19: Filename of the image with the corresponding min/max value pair for the side with the vertical line down.

Filename	Min/Max value of the pixel
m3_wvld	0/8
m3_1vld	0/8
m3_2vld	0/8
m3_3vld	0/8
m3_5vld	0/7
m3_7vld	0/7
m3_4vld	0/8

Comparing side with vertical line up/vertical line down

Comparing the images of both sides with each other it is mentionable that on both sides the radionuclides must be allocated in the same amount. Additionally the kind of radionuclides must be on both sample surfaces the same.

Subtraction of images

See discussion for the SLA sample

7 Literature sources

[Agr 61] Agranovich, V.M.; Semenov, L.P. 1961. Contribution to the theory of radiation effects on some properties of graphite. *Atomic Energy*, 10(6): 572-576.

[Anc 05] Ancius, D.; Ridikas, D.; Remeikis, V.; Plukis, A.; Plukiene, R.; Cometto, M. 2005. Evaluation of the activity of irradiated graphite in the Ignalina Nuclear Power Plant RBMK-1500 reactor. *NUKLEONIKA*, 50(3): 113-120.

[Bak 70] Baker, D.E. 1970. Graphite as a neutron moderator and reflector material. *Nuclear Engineering and Design*, 14: 413-444.

[Bis 01] Bisplinghoff, B.; Lochny, M.; Fachinger, J.; Brücher, H. 2001: Radiochemical characterisation of graphite from Jülich experimental reactor (AVR). In Proceedings Technical Committee Meeting held in Manchester (1999). Nuclear Graphite Waste Management, Vienna.

[Bro 01] Brown, F.J.; Palmer, J.D.; Wood, P. 2001: Derivation of a radionuclide inventory for irradiated graphite-chlorine-36 inventory determination. In Proceedings Technical Committee Meeting held in Manchester (1999). Nuclear Graphite Waste Management, Vienna.

[Bus 02] Bushuev, A.V.; Zubarev, V.N.; Proshin, I.M. 2002. Impurity composition and content in graphite from commercial reactors. *Atomic Energy*, 92(4): 331-335.

[Cau 89] Causey, Rion A. 1989. The interaction of tritium with graphite and its impact on tokamak operations. *Journal of Nuclear Materials*, 162-164: 151-161.

[Che 94] Chebotarev, V.V.; Fomin, I.P.; Pavlichenko, R.O.; Skibenko, A.I.; Tereshin, V.I.; Vojtsenya, V.S. 1994. The prospects of using carbon-graphite materials as construction elements of the microwave plasma diagnostic in a fusion reactor. *Journal of Nuclear Materials*, 212-215: 1157-1162.

[Dip 04] Rüdiger, Jürgen 2004. Dekontaminationsuntersuchungen an Reaktorgraphit mittels Solventextraktion. Diploma Thesis, Dept. of Chemistry and Biotechnology, University of Applied Sciences Aachen, Aachen

[Eng 84] Engle, G.B.; Kelly, B.T. 1984. Radiation Damage of Graphite in Fission and Fusion Reactor Systems. *Journal of Nuclear Materials*, 122&123: 122-129.

[Fis 70] Fischer, Helmut A., and Werner Gottfried 1970. *Autoradiographie*. Walter de Gruyter

[Flo 09] Florjan, Monika W.: *Dekontamination von Nukleargraphit durch thermische Behandlung.* Berichte des Forschungszentrums Jülich (FZJ) – Nr. 4322, ISSN 0944-2952, Jülich, 2009

[Fuk 85] Fukutomi, M.; Fujitsuka, M.; Okada, M. 1985. The development and thermal testing of graphite/carbon bonds for fusion reactor applications. *Journal of Nuclear Materials*, 133-134: 769-772.

[Fro 04] Frolov, V.V.; Kryuchkov, A.V.; Kuznetsov, Yu.N.; Moskin, V.A.; Pankrat'ev, Yu.V.; Romenkov, A.A. 2004. Possibility of burning irradiated graphite from decommissioned nuclear-power generating units. *Atomic Energy*, 97(5): 781-784.

[Gui 10] Guittonneau, F.; Abdelouas, A.; Grambow, B. 2010. HTR Fuel Waste Management: TRISO separation and acid-graphite intercalation compounds preparation. *Journal of Nuclear Materials*, 407: 71-77.

[Gul 64] Gulbransen, E.A.; Andrew, K.F.; Brassart, F.A.; Feild , Jr., A.L. 1964. Ablation of high purity and nuclear reactor core graphite in oxygen and air. *Journal of Nuclear Materials*, 13(1): 40-48.

[Haa 90] Haag, G.; Mindermann, D.; Wilhelmi, G.; Persicke, H.; Ulsamer, W.1990. Development of reactor graphite. *Journal of Nuclear Materials*, 171: 41-48.

[Han 00] Handbuch: Serial Micro Channel SMC 2100 AK/DD/DC. FST Freiberger Sensortechnik GmbH

[Hop 03] Hopkins, K.L.; Marsden, B.J.; Dundulis, G.; Kopustinskas, V.; Liaukonis, M.; Augutis, J.; Uspuras, E. 2003. Prediction of fuel channel – graphite gas gap behaviour in RBMK reactors. *Nuclear Engineering and Design*, 223: 117-132.

[Ia1 06] IAEA 2006. *Characterization, Treatment and Conditioning of Radioactive Graphite from Decommissioning of Nuclear Reactors*, *IAEA-TECDOC-1521*, ISBN 92–0–112006–0, Vienna.

[Ia2 04] IAEA 2004. *Energy supply options for Lithuania*. IAEA-TECDOC-1408, ISBN 92-0-110004-3, Vienna.

[Ish 04] Ishihara, M.; Sumita, J.; Shibata, T.; Iyoku, T.; Oku, T. 2004. Principle design and data of graphite components. *Nuclear Engineering and Design,* 233: 251-260.

[Kar 05] Karlina, O.K.; Klimov, V.L.; Ojovan, M.I.; Pavlova, G.Yu.; Dmitricv, S.A.; Yurchenko, A.Yu. 2005. Immobilization of carbon-14 from reactor graphite waste by use of self –sustaining reaction in the C-Al-TiO2 system. *Journal of Nuclear Materials*, 345: 84-85.

[Kli 61] Klimenkov, V.I.1961. Behavior of graphite in nuclear reactor stacks. *Atomic Energy*, 10(5): 447-460.

[Leb 98] Lebedev, I.G.; Virgil'ev, Yu.S. 1998. Comparative tests of the radiation resistance of reactor graphite. *Atomic Energy,* 85(5)

[Lee 98] Lees, J.E.; Fraser, G.W. 1998. Microchannel plate detectors for ^{14}C autoradiography. *IEEE Transactions on Nuclear Science*. 95(3): 288-1292.

[Lex 06] Lexa, D.; Kropf, A.J. 2006. Thermal, structural and radiological properties of irradiated graphite from the ASTRA research reactor – Implications for disposal . *Journal of Nuclear Materials*, 348: 122-132.

[Mcg 11] McGann, Owen J.; Ojovan, Michael I. 2011. The synthesis of graphite-glass composites intended for the immobilisation of waste irradiated graphite. *Journal of Nuclear Materials*, 413: 47-52.

[Mer 69] Merz, E.; Riedel, H.J.: Spurenverunreinigung in Reaktor-Graphit. Arbeit ausgeführt bei der Kernforschungsanlage Jülich des Landes Nordrhien-Westfalen e.V., Assoziation-Nr.: 003-63-1 RGAD, 1969, Mikrofilm

[Moo 08] Moormann, Rainer; Hinssen, Hans-Klemens; Kühn, Kerstin; Schlögl, Bärbel; Fechter, Mary; Mitchell, Mark 2008. Oxidation experiments and theoretical examinations on graphite materials relevant for the PBMR. *Nuclear Engineering and Design,* 238: 3018-3025.

[Ned 11] Nedveckaite, Tatjana; Marciulioniene, Danute; Mazeika, Jonas; Paskauskas, Ricardas 2011. Radiological and Environmental Effects in Ignalina Nuclear Power Plant Cooling Pond – Lake Druksiai: From Plant put in Operation to Shut Down Period of Time. *Nuclear Power – Operation, Safety, Environment*, ISBN 978-953-307-507-5

[Nei 07] Neighbour, G.B.(Ed.) 2007. *Management of Ageing in Graphite Reactor Cores.* Cambridge: RSC Publishing. ISBN 978-0-85404-345-3

[Neu 87] Neumüller, O.A. 1987. *Römpps Chemie Lexikon*, 5: 3471-3472, Stuttgart

[Pan 08] Panyukov, S.V.; Subbotin, A.V. 2008. Theory of radiation induced shape change of graphite. *Atomic Energy*, 105(1): 32-41.

[Puz 10] Puzas, A.; Remeikis, V.; Ezerinskis, Z.; Serapinas, P.; Plukis, A.; Duskesa, G. 2010. *MASS* SPECTROMETRIC DETERMINATSION OF IMPURITIES IN REACTOR CORE GRAPHITE FOR RADIOACTIVE WASTE COMPOSITION MODELLING. *Lithuanian Journal of Physics*, 50(4): 445-449.

[Röd 76] Rödig, M.; Kleist, G.; Schiffers, H.; Nickel, H. 1976. *Zur bruchmechanischen Untersuchung von Reaktorgraphit.* Berichte der Kernforschungsanlage Jülich – Nr.1275, Jülich

[Sap 79] Sappok, R. 1979. Diamantsynthese. *Chemie in unserer Zeit*, 4(5): 145-151.

[Sgl 1] Information due to contact with the company SGL Carbon

[Sri 08] Srinivasan, M. 2008. On estimating the fracture probability of nuclear graphite components. *Journal of Nuclear Materials*, 381: 185-198.

[Sub 06] Subbotin, A.V.; Ivanov, O.V.; Dremin, I.M.; Shevel´ko, V.P.; Nechitailo, V.A.; Zolotarev, K.I. 2006. Primary radiation defect to graphite in different types of reactors. *Atomic Energy*. 100(3): 199-209.

[Tuc 03] Borchard-Tuch, C. 2003. Lithium-Ionen-Akkus. *Chemie in unserer Zeit*, 37(6): 436-437.

[Dip 04] Rüdiger, Jürgen 2004. Dekontaminationsuntersuchungen an Reaktorgraphit mittels Solventextraktion. Diploma Thesis, Dept. of Chemistry and Biotechnology, University of Applied Sciences Aachen, Aachen

[Vil 03] Vilser, F. 2003. *Quantifikation digitale Autoradiographie im kerntechnischen Strahlenschutz*. Diploma Thesis, University of Applied Sciences Munich, Munich

[Vre 08] Vreeling, J.A.; Wouters, O.; Laan, J.G. van der 2008. Graphit irradiation testing for HTR technology at the High Flux Reactor in Petten. *Journal of Nuclear Materials*, 381: 68-75.

[Wis 01] Wise, M. 2001: *Management of UKAEA graphite liabilities*. In Proceedings Technical Committee Meeting held in Manchester (1999). Nuclear Graphite Waste Management, Vienna.

[Www 1] http://www.nucleartourist.com

[Www 2] http://www.kernfragen.de/kernfragen/lexikon/t/thermische_saeule.php

[Www 3] http://www.francenuc.org/en_sites/cen_sain_e.htm